AD-A055 943 LOCKHEED MISSILES AND SPACE CO INC PALO ALTO CALIF PA--ETC F/G 7/4
ATMOSPHERIC CO2 INFRARED BACKGROUND INVESTIGATION. EXPERIMENTAL--ETC(U).
DEC 77 J B KUMER, T C JAMES DNA001-77-C-0190
UNCLASSIFIED LMSC-D566309 DNA-4409F NL

| OF |
ADA
055943

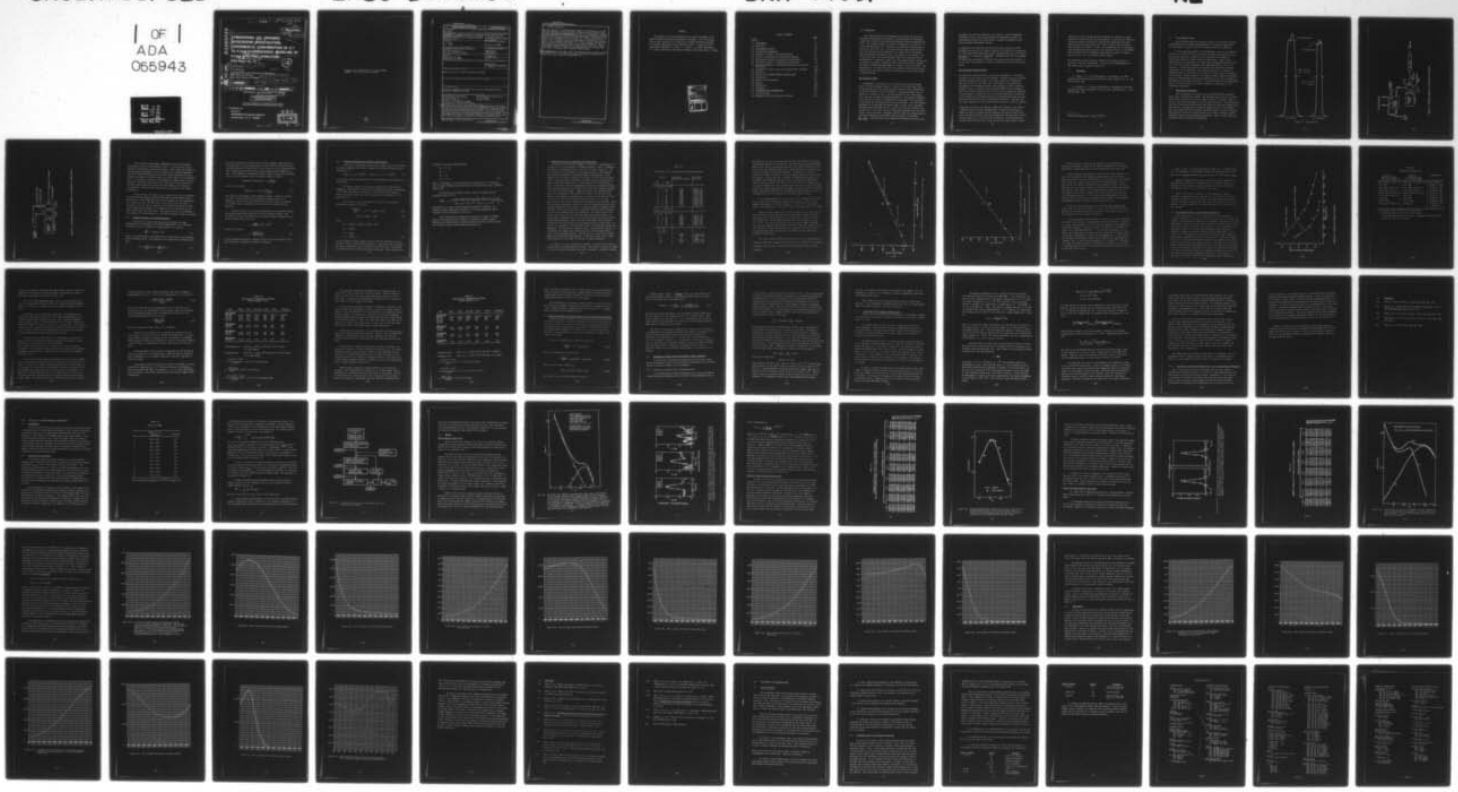

END
DATE
FILMED
8-78
DDC

(6)

ATMOSPHERIC CO_2 INFRARED BACKGROUND INVESTIGATION. EXPERIMENTAL CONFIRMATION OF 2.7 TO 4.3 μm FLUORESCENCE; MODELING OF 4.3 μm SPECTRAL STRUCTURE.

micrometers

(12)

HAES Report No. 70

HAES-70

(10) J.B. Kumer
T.C. James

Lockheed Palo Alto Research Laboratory
3251 Hanover Street
Palo Alto, California 94304

(14) LMSC-D566309,
DNA-HAES-70

(11) Dec [redacted] 77

(12) 78p.

(9) Final Report. [redacted] 11 May [redacted] —31 Dec [redacted] 77,

CONTRACT No. DNA 001-77-C-0190

(15)

APPROVED FOR PUBLIC RELEASE;
DISTRIBUTION UNLIMITED.

THIS WORK SPONSORED BY THE DEFENSE NUCLEAR AGENCY
UNDER RDT&E RMSS CODE B322077464 S99QAXHI00427 H2590D.

Prepared for
Director
DEFENSE NUCLEAR AGENCY
Washington, D. C. 20305

210 118

Destroy this report when it is no longer needed. Do not return to sender.

UNCLASSIFIED

SECURITY CLASSIFICATION OF THIS PAGE *(When Data Entered)*

REPORT DOCUMENTATION PAGE

READ INSTRUCTIONS BEFORE COMPLETING FORM

1. REPORT NUMBER: DNA 4409F	2. GOVT ACCESSION NO.
3. RECIPIENT'S CATALOG NUMBER	
4. TITLE *(and Subtitle)*: ATMOSPHERIC CO_2 INFRARED BACKGROUND INVESTIGATION: EXPERIMENTAL CONFIRMATION OF 2.7 to 4.3 μm FLUORESCENCE; MODELING OF 4.3 μm SPECTRAL STRUCTURE HAES Report No. 70	5. TYPE OF REPORT & PERIOD COVERED: Final Report for Period 11 May 77—31 Dec 77
	6. PERFORMING ORG. REPORT NUMBER: LMSC D566309
7. AUTHOR(s): J. B. Kumer, T. C. James	8. CONTRACT OR GRANT NUMBER(s): DNA 001-77-C-0190
9. PERFORMING ORGANIZATION NAME AND ADDRESS: Lockheed Palo Alto Research Laboratory, 3251 Hanover Street, Palo Alto, California 94304	10. PROGRAM ELEMENT, PROJECT, TASK AREA & WORK UNIT NUMBERS: NWED Subtask S99QAXHI004-27
11. CONTROLLING OFFICE NAME AND ADDRESS: Director, Defense Nuclear Agency, Washington, D.C. 20305	12. REPORT DATE: December 1977
	13. NUMBER OF PAGES: 84
14. MONITORING AGENCY NAME & ADDRESS *(if different from Controlling Office)*	15. SECURITY CLASS *(of this report)*: UNCLASSIFIED
	15a. DECLASSIFICATION/DOWNGRADING SCHEDULE

16. DISTRIBUTION STATEMENT *(of this Report)*

Approved for public release; distribution unlimited.

17. DISTRIBUTION STATEMENT *(of the abstract entered in Block 20, if different from Report)*

18. SUPPLEMENTARY NOTES

This work sponsored by the Defense Nuclear Agency under RDT&E RMSS Code B322077464 S99QAXHI00427 H2590D.

19. KEY WORDS *(Continue on reverse side if necessary and identify by block number)*

Nuclear Optical Interference
CO_2 Fluorescence 2.7 to 4.3 μm
Quenching of CO_2 (ν_3)
CO_2 (ν_3) to N_2^+ Vibration Transfer
Infrared CO_2 4.3 μm Aurora and Airglow
Nuclear Enhanced Atmospheric CO_2
4.3 μm Radiance
DNA/AFGL Infrared

20. ABSTRACT *(Continue on reverse side if necessary and identify by block number)*

The High Altitude Effects Simulation (HAES) Program sponsored by the Defense Nuclear Agency since the early 1970 time period, compromises several groupings of separate, but interrelated technical activities, e.g., ICECAP (Infrared Chemistry Experiments-Coordinated Auroral Program). Each of the latter have the common objectives of providing information ascertained as essential for the development and validation of predictive computer codes designed for use with high priority DoD radar, communications, and optical defensive systems.

DD FORM 1 JAN 73 1473 EDITION OF 1 NOV 65 IS OBSOLETE

UNCLASSIFIED

SECURITY CLASSIFICATION OF THIS PAGE *(When Data Entered)*

20. ABSTRACT (Continued)

Since the inception of the HAES Program, significant achievements and results have been described in reports published by DNA, participating service laboratories, and supportive organizations. In order to provide greater visibility for such information and enhance its timely applications, significant reports published early calendar 1974 shall be identified with an assigned HAES serial number and the appropriate activity acronym (e.g., ICECAP) as part of the report title. A complete and current bibliography of all HAES reports issued prior to and subsequent to HAES Report No. 1, dated 5 February 1974 entitled, "Rocket Launch of an SWIR Spectrometer into an Aurora (ICECAP 72)," AFCRL Environmental Research Paper No. 466, is maintained and available on request from DASIAC, DoD Nuclear Information and Analysis Center, 816 State Street, Santa Barbara, California 93102, Telephone (805) 965-0551.

This report, which is the final report under DNA Contract No. DNA 001-76-C-0190 is the 70th report in the HAES series. It documents work performed in the period 11 May 1977 through 31 December 1977.

PREFACE

The success of the work reported here was crucially dependent on the generous advice and discussion provided by colleagues. All of the people that we dealt with went out of their way to provide information pertinent to successful performance of the contractual tasks. To name just a few, these people included A. T. Stair, C. A. Blank, J. C. Ulwick, Ned Wheeler, R. D. Sears, Aiden Roche, John Kemp, Tom Condron, Phil Doyle, and D. J. Baker.

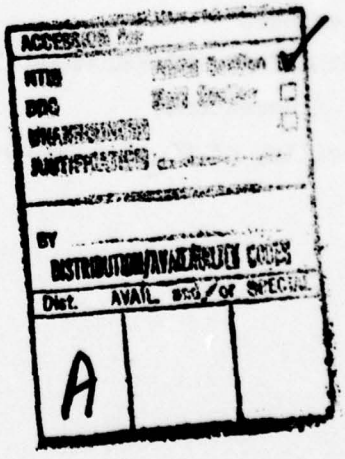

TABLE OF CONTENTS

1.0 INTRODUCTION

This report describes the performance of laboratory and field data evaluation efforts which are relevant to the DNA program for developing capability to predict nuclear-enhanced atmospheric infrared background radiance. The laboratory effort was aimed at confirmation of the CO_2 2.7 to 4.3 μm fluorescence process. This process is expected to be important in the nuclear case (Ref. 1-1); it also has bearing on the possibility that CO_2 2.7 μm emission may be responsible for a long-lived 2.7 μm auroral emission component that Mitchell (Ref. 1-2) believes to be present in the 2.7 μm aurora data. The data evaluation effort was concerned with the development of a capability to model CO_2 4.3 μm zenith spectral radiance and to validate this model by comparison with 4.3 μm zenith spectral radiance obtained via rocket-borne measurements on 3/24/73, 4/11/74 and 4/1/76. The development of a reliable model for this prediction of auroral and nuclear-induced 4.3 μm CO_2 spectral radiance is necessary for the rational design of advanced systems.

The Laboratory Effort

Measurements of the CO_2 2.7 to 4.3 μm fluorescence were performed using a variable frequency chopper to chop the 2.7 μm light which enters the fluorescence cell and a phase sensitive amplifier and an InSb detector to sense the resultant 4.3 μm fluorescence. These measurements were performed for a variety of CO_2, Ar, He and N_2 mixtures in the fluorescence cell, and with a variety of chopping frequencies. The frequency dependence of the fluorescent signal is determined by the frequency of the exciting 2.7 μm signal and the decay time for CO_2 ν_3 excitation. From the frequency dependence of the observed fluorescent signal, we were able to determine quenching rate coefficients for CO_2 (ν_3) by Ar and He and vibration transfer from CO_2 (ν_3) to N_2[‡] that are in reasonable agreement with literature values; we were also able to determine that the signal is essentially due to resonance fluorescence ($001 \longrightarrow 000$) rather than direct fluorescence ($\begin{matrix}011\\101\end{matrix} \longrightarrow \begin{matrix}020\\100\end{matrix}$). Cooled and uncooled transmission measurements utilizing a CO_2

absorption cell were also performed in an attempt to provide independent confirmation of the latter point; problems of experimental geometry and interpretation remain to be solved before a definite confirmation can be drawn from these measurements, however.

In addition to our laboratory work with the present apparatus, we have determined that the use of a powerful tunable 2.7 μm laser will be necessary to obtain quantitative measurement of the branching ratio for 4.3 μm emission $\left(\begin{smallmatrix}021\\101\end{smallmatrix}\rightarrow\begin{smallmatrix}020\\100\end{smallmatrix}\right)$ vs. 2.7 μm emission $\left(\begin{smallmatrix}021\\101\end{smallmatrix}\rightarrow 000\right)$. A chromatix CMX-4 dye laser pumping an $LiNbO_3$ optical parametric oscillator with piezo electric fine tuning of the dye laser cavity appears to provide a satisfactory 2.7 μm tunable laser system.

The Field Data Evaluation Effort

The field data evaluation effort involved the development of a capability to model CO_2 4.3 μm zenith spectral radiance. The model requires a detailed radiation transport calculation of the zenith radiance in approximately 2420 lines in 11 CO_2 (ν_3) bands, and a convolution of the appropriate instrumental slit function over these line radiances in order to generate synthetic spectra. Agreement with rocket-borne SWIR CVF data obtained on 3/24/73 in an auroral break up and on 4/11/74 in quiet night time conditions was good enough to confirm that CO_2 is the emitter principally responsible for the observed 4.3 μm feature and that we reasonably understand the quiet night time and the auroral CO_2 4.3 μm emission mechanisms. Features that may appear longward of 4.5 μm in the CVF data are due to "cold" CO_2 emission.

Preliminary application with regard to HIRIS data obtained 1 April 1976 in a moderate aurora has shown that HIRIS-like resolution is sufficient to observe the optical thickness induced change in the spectral shape of the CO_2 4.3 μm auroral feature as the rocket penetrates through the 80 to 110 km altitude region; just a small fraction of auroral or nuclear-induced CO_2 emission above 80 km will occur in the red and blue spike regions; nuclear

deposition at lower altitudes should be expected to contribute to nadir radiance in both the red and blue spike regions; and finally that HIRIS-like resolution should be sufficient to identify the 626*001-000 band origin, and the 626 011-010 band origin and Q branch in zenith spectral radiance data obtained at altitudes $z \leq 70$ km. We recommend that the 4.3 μm spectral model be improved by the inclusion of the emitters NO^+, N_2O, CO and $^{14}N^{15}N$. The model should also be extended to other spectral regions of interest, such as the 2.7, 5.3, 6.3 and LWIR spectral regions.

The Laboratory and data evaluation efforts are described in detail in Sections 2.0 and 3.0, respectively. Conclusions and recommendations for the overall project appear in Section 4.0.

1.1 References

1-1 Kumer, J. B., '4.3 um Measurements,' Proceedings of the HAES Infrared Data Review Meeting held 12-15 June 1977, Falmouth, Mass., p. 291, AFGL-OP-TM-05, 1977.

1-2 Mitchell, H., 'Another Interpretation,' Proceedings of the HAES Infrared Data Review Meeting held 13-15 June 1977, Falmouth, Mass., p. 327, AFGL-OP-TM-05, 1977.

*Here 626 designates the isotope $^{16}O^{12}C^{16}O$

2.0 THE LABORATORY EFFORT

The laboratory effort has included a number of measurements directed toward gaining a more detailed understanding of the processes important in the fluorescence of CO_2 at 4.3 μm when irradiated with 2.7 μm radiation.

We have made measurements of the transmission of the 4.3 μm radiation through a cell filled with CO_2 with several different concentrations of CO_2 and rare gas perturber. Studies have also been made of the change in fluorescence signal with various amounts of added gases. These results indicated that our measurements were being made at chopping frequencies which were of the same order of magnitude as the quenching rates for the 4.3 μm radiation. A considerable effort has therefore been directed at obtaining measurements of the magnitude of the fluorescence signal as a function of chopping frequency. These data can be analyzed to yield values for quenching rate constants. Further studies of the change in signal produced with various amounts of added Nitrogen have provided information on the rate of transfer of vibrational energy between CO_2 and N_2. A brief description of the experimental setup is given below which will then be followed by a description of the individual measurements.

2.1 Experimental Arrangement

These measurements were made using an Infrared Industries Blackbody Source with a variable speed chopper. The blackbody source had a 2.7 μm filter placed after the chopper so that the output consisted of a chopped signal at 2.7 μm. This signal irradiated a 2 cm long fluorescence cell. The fluorescence cell had a 4.3 μm filter placed at the exit window, and this was followed by an InSb detector. The detector was therefore seeing just the 4.3 μm radiation which is produced and not the original excitation signal at 2.7 μm. Figure 2-1 shows spectra of the 2.7 μm filter and the 4.3 μm filter. Figure 2-2 shows a schematic diagram of the experimental arrangement. Figure 2-3 also shows the arrangement used in absorption measurements.

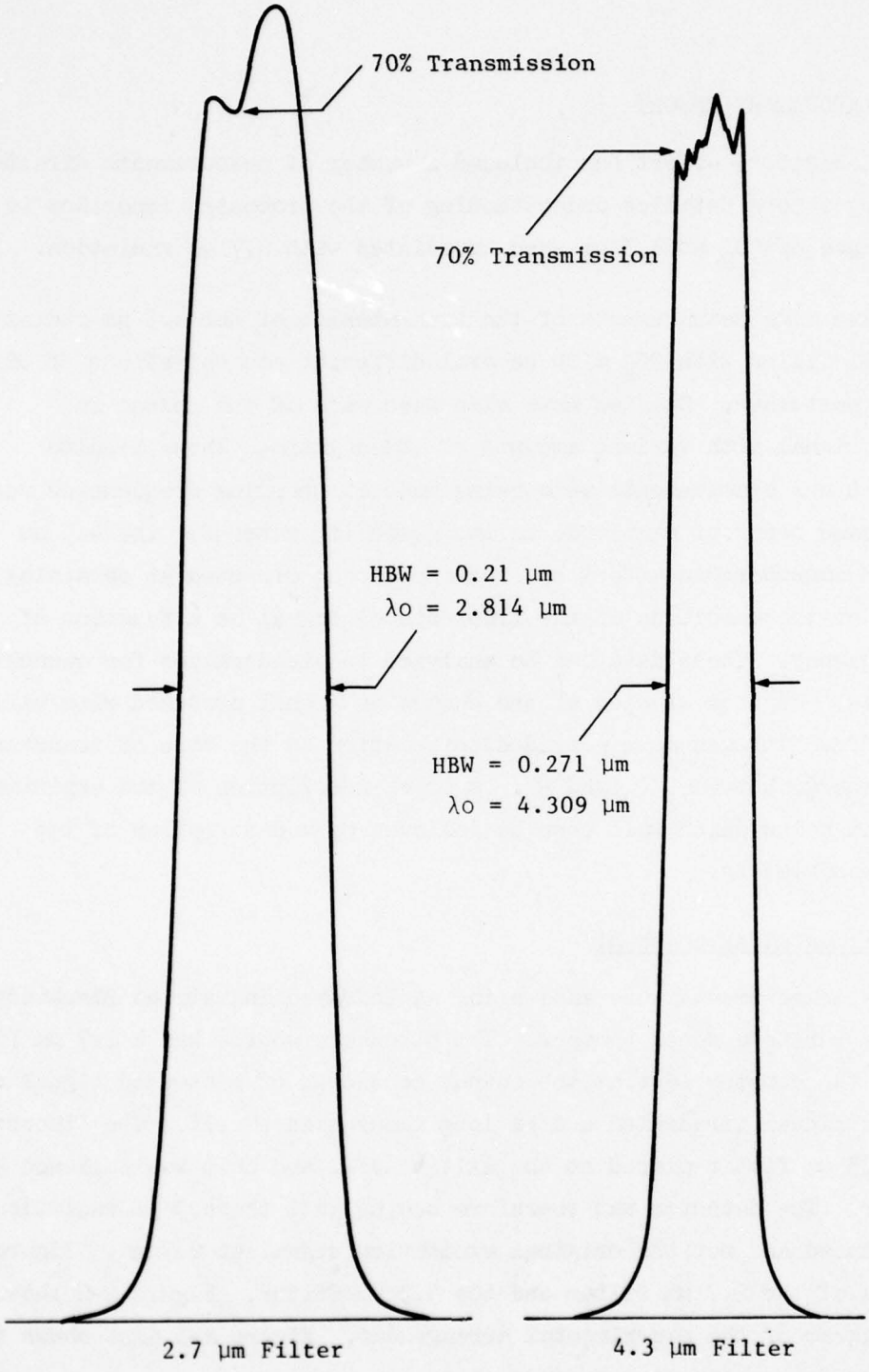

Figure 2-1 Filter Spectra

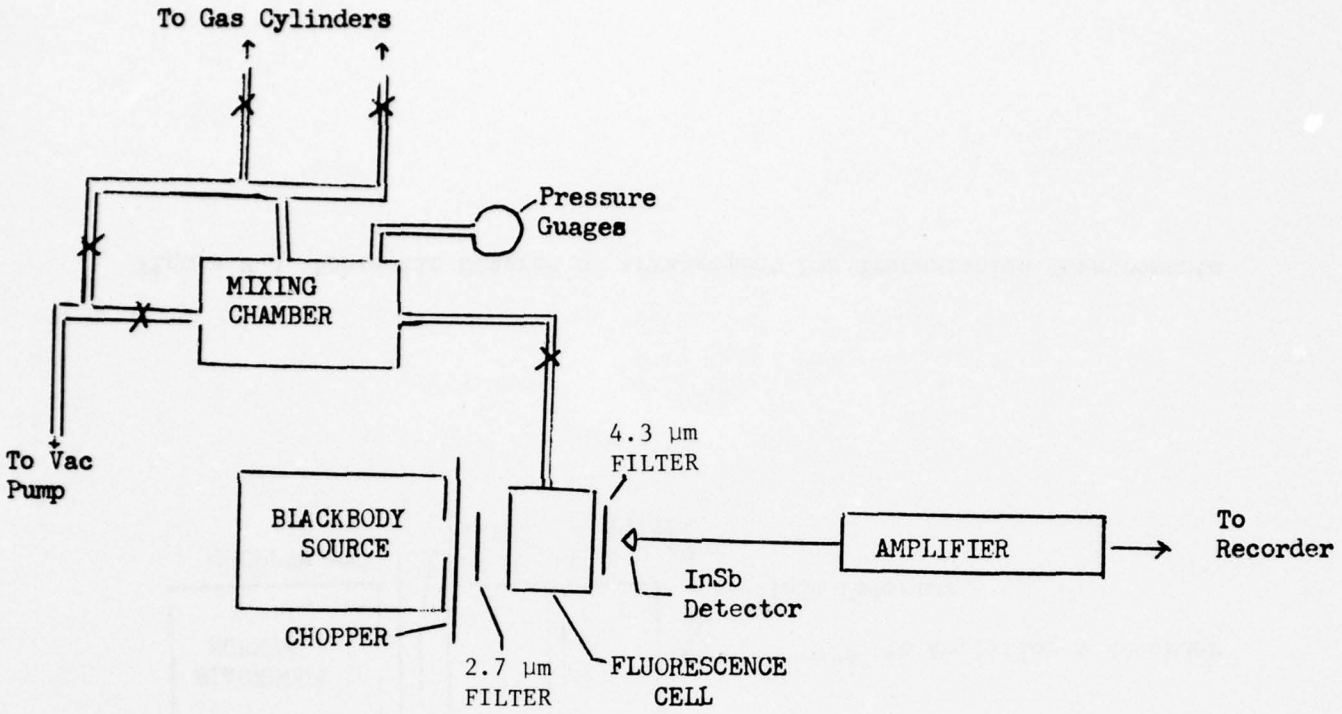

Figure 2-2 Schematic Diagram of Fluorescence Experiment

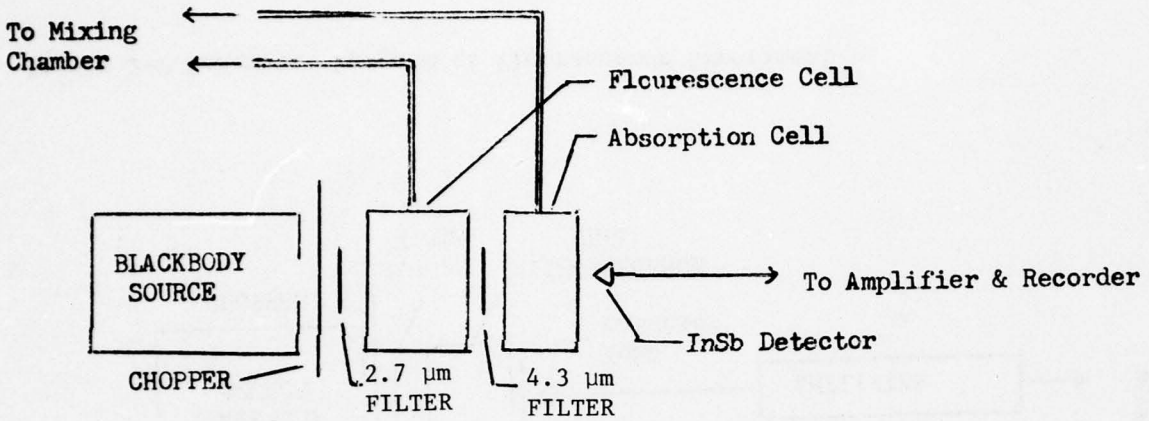

Figure 2-3 Schematic Diagram of Arrangement for Transmission Measurements

In our earlier report (James, DNA4238F) we reported transmission measurements in which a long absorption cell of ~ 16 cm length was placed between the fluorescence cell and the detector. After making some changes in our experimental arrangement we were no longer able to obtain measurements with this configuration and had to use a much shorter absorption cell which enabled us to place the detector closer to the exit window of the fluorescence cell. We are unable to account for the reduction in signal which we are now observing. This may be due in part to the fact that the same detector was not used, and may also be due to the fact that changes in our setup have eliminated some scattered light which may have been present in our earlier measurements.

We have looked at the shape of the excitation pulse and the resulting 4.3 μm fluorescence signal using a PAR model TDH-9 Waveform Eductor and an X-Y recorder. These measurements show that the signals are well approximated by a single sine wave. The fact that we have nearly a pure sine wave is traceable to the fact that the opening in the blackbody source and the width of the chopper blade openings are of comparable size so that there is not a sharp on-off square wave type source. This turns out to be very convenient in that response of the fluorescence to a sine wave excitation is easy to calculate.

2.2 Response of System to Sine Wave Excitation

The fact that we have a sine wave excitation leads to a simple expression for the magnitude of the observed fluorescence. For a sine wave excitation the rate of formation of excited species n* is given by

$$\frac{dn^*}{dt} = A \sin \omega t - kn^* \qquad 2\text{-}1$$

where k is the reciprocal of the lifetime and A is determined by the amplitude of the excitation source. The solution of this equation can be written in the form

$$n^* = \frac{Ak}{k^2+\omega^2} \sin \omega t - \frac{aw}{k^2+\omega^2} \cos \omega t \qquad 2\text{-}2$$

This form of writing the solution shows that the resultant signal which will be proportional to n* can be expressed as a factor which is in phase with the excitation source and a factor which is out of phase with the excitation source. This is particularly convenient when a phase sensitive lock-in amplifier is used. If the amplifier is adjusted to measure signals in phase the exciatation source, then the amplitude of the fluorescence signal is given by

$$\text{Amplitude of Fluorescence} = \frac{Ak}{k^2 + \omega^2} \qquad 2\text{-}3$$

which can be written as

$$\text{Fluorescence} = S(0)\,\frac{1}{1 + (\omega/k)^2} \qquad 2\text{-}4$$

where S(0) is the amplitude at zero chopping frequency: Therefore, the fall off of the in phase component with increasing chopping frequency is a Lorentzian. Note that the term involving Cos ωt in Eq. (2-2) is 90 degrees out of phase with the excitation source and will not be detected by the amplifier.

From Eq. (2-4) it is clear that measurements of the frequency response of the fluorescent signal yield values for the quenching lifetime. From Eq. (2-4), the ratio of the signal at two different chopper frequencies can be used to extract a decay rate k by:

$$k = \frac{2\pi}{\sqrt{R - 1}}\,(f_2^{\,2} - Rf_1^{\,2})^{\frac{1}{2}} \qquad 2\text{-}5$$

where R is the ratio:

$$R = \frac{\text{Signal at } f_1}{\text{Signal at } f_2} \qquad 2\text{-}6$$

In the following discussion we consider the way in which the response of the CO_2 fluorescence is modified by addition of Nitrogen.

2.3 Transfer of Excitation in Collision with Nitrogen

Fluorescence measurements made when N_2 is added to CO_2 can be utilized to obtain information on the rate of transfer of excitation between CO_2 and Nitrogen due to

$$CO_2(\nu_1, \nu_2, \nu_3) + N_2(v=0) = CO_2(\nu_1, \nu_2, \nu_3 - 1) + N_2(v=1) \qquad 2\text{-}7$$

In this case a simple Lorentzian decay of the fluorescence with frequency is not obtained.

We indicate briefly the form of the solution when reaction (7) is considered. This analysis is more easily performed using complex exponentials $A\, e^{i\omega t}$ rather than sine wave excitation. The results will be identical, however, as we will simply pick out the portion of the solution that is in phase with $e^{i\omega t}$.

In the case of a $CO_2 + N_2$ mixture we will have two simultaneous differential equations of the form:

$$\frac{d(CO_2)^*}{dt} = A\, e^{i\omega t} - k_a(CO_2)^* + k_b N_2^* \qquad 2\text{-}8a$$

$$dN_2^* = k_c(CO_2)^* - k_d N_2^* \qquad 2\text{-}8b$$

where:

$$k_a = k_1(CO_2) + k_2(N_2) + k_7(N_2) + k_3(M)$$

$$k_b = k_7(CO)_2$$

$$k_c = k_7(N_2)$$

$$k_d = k_7(CO_2) + Q \qquad 2\text{-}9$$

In these equations $k_1(CO_2)$, $k_2(N_2)$ and $k_3(M)$ represent quenching of 4.3 μm radiation by CO_2, N_2, and any other added gas. $k_7(N_2)$ and $k_7(CO_2)$ represent the energy transfer rate due to reaction (7) and its reverse. Q represents the quenching of N_2^* by collision with other molecules. These equations can

be written in the more convenient form:

$$k_a = k + vx$$

$$k_b = v$$

$$k_c = vx$$

$$k_d = v + q \qquad 2\text{-}10$$

where $x = [N_2]/[CO_2]$, v is the forward rate of reaction (7), k is the total rate of $(CO_2)\nu_3$ excluding reaction (7) and Q is the quenching of N_2^*, excluding reaction (7).

The portion of the solution to Eqs. 8 which is in phase with the excitation term $A\, e^{i\omega t}$ is

$$(CO_2)^* = A\, e^{i\omega t}\left[\frac{(v+q)(vk+qvx+qk-w^2)+\omega^2(q+k+v+vx)}{(vk+qvx+qk-\omega^2)^2+\omega^2(q+k+v+vx)^2}\right] \qquad 2\text{-}11$$

This result is no longer a simple Lorentzian function of frequency. By suitably choosing experimental conditions, the frequency dependence can be utilized to obtain information on the rate v.

The following section summarizes the results of a number of measurements in which quenching rate constants are obtained in mixtures without Nitrogen and in which Nitrogen containing mixtures are used to extract a value for the energy transfer rate constant for reaction (7).

2.4 Experimental Results of Quenching Rate Measurements

In this section we provide a summary of the results of measurements of intensity of the 4.3 μm emission vs chopping frequency. Table 2-1 summarizes the results of measurements made on CO_2 + Ar, CO_2 + He, and pure CO_2 The total pressure of each component of the mixture is given. The resulting decay constant obtained by a regression analysis which performs a least squares fit of the data to equation 2-4 is given. We also list the average value of the decay constant calculated from utilizing every data point of a given run and calculating values of k from equation 2-5 for every pair of points. This value is given in parentheses followed by a standard deviation about this average value. We consider the results of the regression analysis to be the more reliable number. Comparison of those two different values gives a good indication of the quality of the data. In a few cases the results of the regression analysis were not available at the time of writing of this report and only the average calculated from eq. 2-5 is listed. Fig. 2-4 shows a plot of the decay rates for mixtures of CO_2 and Argon. While the data shows considerable scatter, the trend of increasing decay rate with increasing pressure of Ar is evident. A few of the points are marked with an asterisk. These points clearly show considerable deviation from the nearly linear relation between decay rate and pressure. The source of these deviations is not clear, but we do feel that these points are unreliable. We include them to indicate that we have occasionally experienced some problems in obtaining reproducible results, and that even though a good fit may be obtained for a given run, the result may agree poorly with similar runs. In some of our experiments we have observed a drift in the observed intensity and background. In some cases we found the source of this difficulty was due to an unstable power supply used in generating the reference signal caused a drift in the observed intensities. The two scans at 5 and 10 Torr of Argon marked with an asterisk showed evidence of this type of drift and it seems likely that this is the source of the error in these measurements.

In figure 2-4 we have indicated two straight lines which can be drawn to yield a value of the quenching rate constant. One of these is drawn to attempt to fit all of the points (except those with an asterisk). Looking at the pure

Table 2-1

Decay Rates of 4.3 μm Emission For Various Gas Mixtures

Mixtures		Decay Rate (Regression Analysis)	Decay Rate (Eq. 2-5)
CO_2 + Argon			
Torr CO_2	Torr Argon		
1	10	1556	1558 ± 139
1	20	2554	2512 ± 704
2	5	2734	2738 ± 170
2	5	1585	1743 ± 378
2	10	3091	3033 ± 267
2	10	1732	1589 ± 202
2	20	2302	2135 ± 279
2	20	2180	2162 ± 256
2	40	3212	3231 ± 126
2	40	3249	3238 ± 269
CO_2 + Helium			
Torr CO_2	Torr He		
2	5	1951	1907 ± 374
2	10	2187	1994 ± 356
2	20	3281	3165 ± 377
2	20	2831	2721 ± 310
2	40	4580	4552 ± 567
1	20	2898	2770 ± 306
Pure CO_2			
Torr CO_2			
2		1382	(1393 ± 152)
2		2102	(2123 ± 74)
2			1569
1		1210	(1382 ± 352
1/2		1229	(1405 ± 571)

CO_2 results at the end of table 2-1 does not show any evident trend in decay constant with pressure at low pressures. The uncertainty of the measurements plus the fact that at low pressures there are other effects limiting the lifetime such as wall collisions makes these results difficult to interpret without more detailed and accurate measurements. Similarly, there is some indication in figure 2-4 that the decay rate may not change very much at low Ar pressures. In this case also, it may be that adding small amounts of Ar may inhibit wall collisions and also increase quenching by a compensating amount so that the slope of the decay rate vs pressure of Ar at higher pressure may not apply in the lower pressure range. We therefore, also have drawn a line on the figure which connects the points at 20 and 40 Torr Ar. This may yield a more accurate value of the quenching rate constant due to the fact that wall effects are not important in this higher pressure range.

The resulting values of k are $k = 1.42 \times 10^{-15}$ utilizing all the points and $k = 1.52 \times 10^{-15}$ utilizing the higher pressure points. These results compare favorably with literature values of $k = 2.52 \times 10^{-15}$ reported by Rosser et al. (1968) and $k = 1.75 \times 10^{-15}$ reported by Stephenson et al. (1971).

Figure 2-5 shows a plot of the results for CO_2 + He. In this case we have less data, and have just drawn a line which gives a good fit to all of the points. The resulting value of the quenching rate constant for He is 2.34×10^{-15} which can be compared with the value by Stephenson et al. of 3.1×10^{-15}. It is also interesting to note that if we compare quenching rate constants obtained using all of the points in figure 2-4 and 2-5, the He rate constant is larger than the Argon rate constant by the ratio 1.72 in excellent agreement with the value of 1.65 obtained for this ratio from Stephenson's measurements.

The decay constants which we have measured are for the total loss of ν_3 emission of CO_2 and are dominated by transfers of ν_3 excitation into ν_1 and ν_2 vibrations. This is also the case with the measurements of Rosser and of Stephenson.

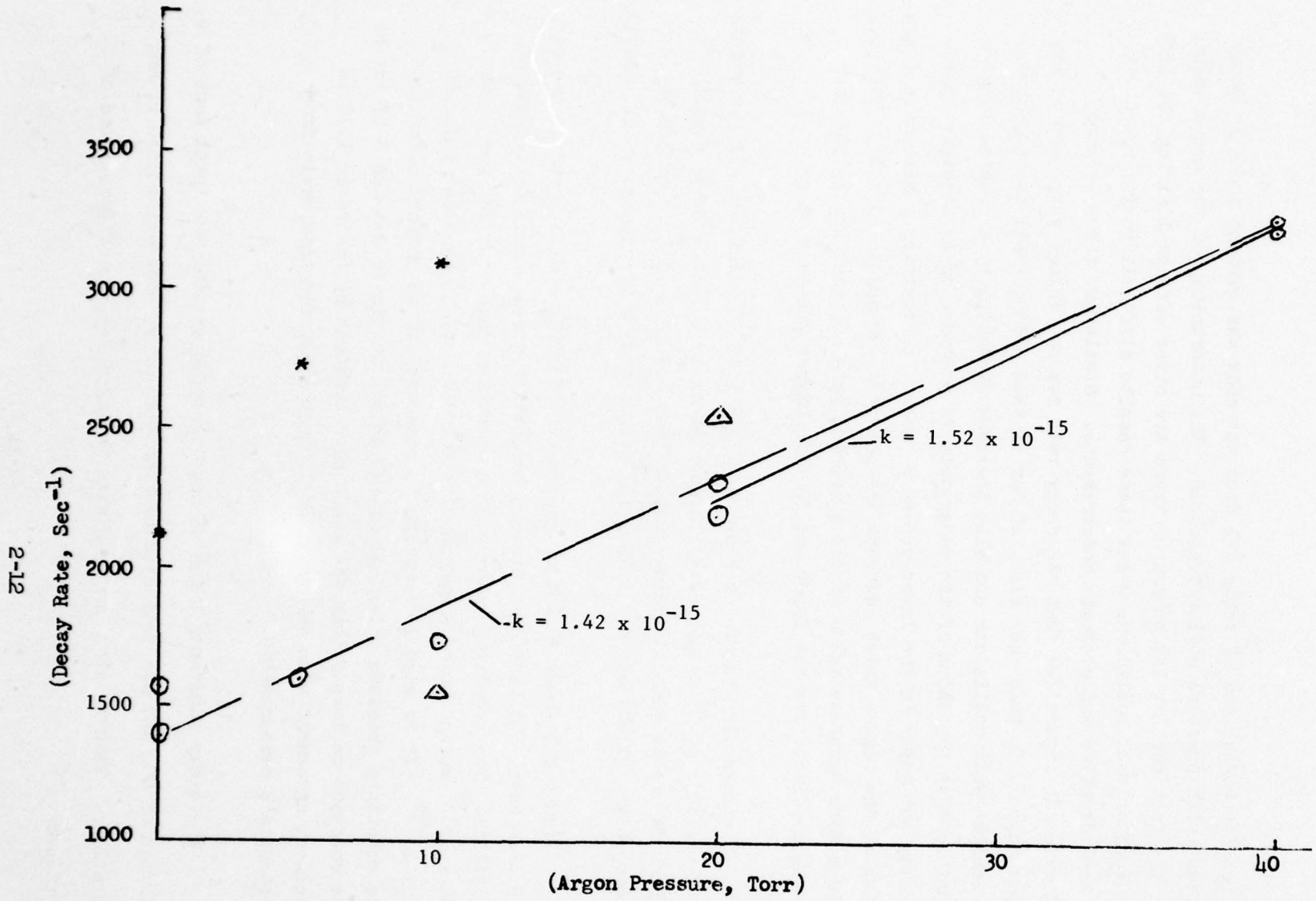

Figure 2-4 Decay Rate vs Argon Pressure (⊙ 2 Torr CO_2, △ 1 Torr CO_2)

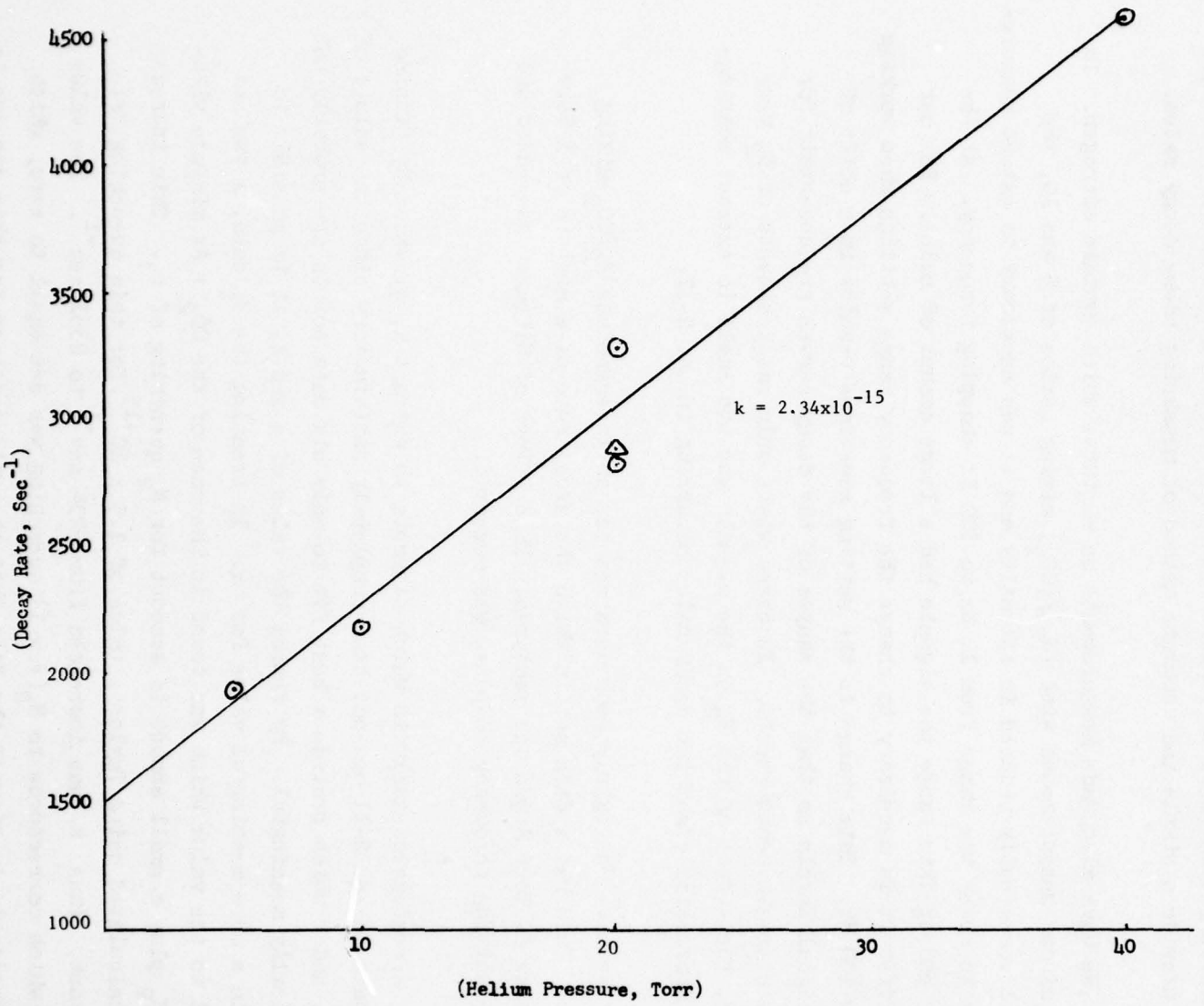

Figure 2-5 Decay Rate vs Helium Pressure (θ 2 Torr CO_2, Δ 1 Torr CO_2)

While our present results for the quenching rate constants must be considered preliminary, we believe that further refinements of our technique will provide a simple and accurate method of measuring these decay rates.

We have also made measurements on mixtures which contain nitrogen. In some of our measurements with $[N_2]/[CO_2]$ mixing ratios of 5 and 10, the signal was greatly reduced in intensity and it was necessary to extend measurements to cover the range from 10 Hz to 300 Hz chopping frequency. At the lower end of this range the signals had a large amount of noise. For our amplifier it is necessary to change the frequency range settings when working below 100 Hz. This change in the setting sometimes results in a shift of the signal levels so that the shapes of the decay curves are uncertain for these nitrogen measurements. In cases where only small amounts of N_2 were added, the effect of the N_2 on the signals was too small to extract meaningful information about the decay rates occurring in eq. 2-11.

We have one fairly good data set for an intermediate N_2/CO_2 mixing ratio. This was a data set in which the decay rate of a mixture of 1 Torr CO_2 plus 20 Torr Argon was measured. Then 2 Torr of Nitrogen was added and the resulting frequency response was measured.

A regression analysis which attempts to extract k, q, and v by fitting the data to eq. 2-11 has not been completely satisfactory since the values of k, q, and v which provide a best fit to only six data points are probably not physically meaningful. By fixing the value of q and k, it is possible to obtain a more meaningful value for v. In treating the N_2 data, k was set equal to the value which was found in the case of the CO_2 + Ar mixture without N_2 plus a small amount to account for N_2 quenching of ν_3. This increase was calculated using Taylor's value of 1.5×10^{-15} for this quenching rate constant. Thus k was increased from 2254 sec^{-1} to 2361 sec^{-1}. The value of q which corresponds to $N_2(v = 1)$ quenching was set equal to zero, which is reasonable in view of the fact that the rate constant for this process is of the order 10^{-20} or less.

With k and q fixed as described, the value of v is 2.827×10^{4} sec^{-1} corresponding to a vibrational transfer rate constant of 8.67×10^{-13} which is in reasonable agreement with the value of 6×10^{-13} given by Taylor.

Figure 2-6 illustrates the manner in which the data is changed by the addition of N_2. These curves clearly indicate the change in shape and magnitude of the intensity vs chopping frequency curves and also indicate the quality of the fits to the data in the two cases.

Before we can report a value of v with confidence it will be necessary to study many more $N_2 + CO_2$ mixtures. We do feel that this is a promising technique for measuring the $CO_2 - N_2$ vibrational energy transfer rate and that further experimental measurements and refinements of the data analysis techniques should lead to reliable values for the energy transfer rate constant.

2.5 Experimental Results of Transmission Measurements

Several measurements of the transmission of the CO_2 fluorescence through a CO_2 filled cell were made. For these measurements the fluorescence cell of 2 cm path length was followed by an absorption cell with 1.5 cm. The experimental arrangement used for this measurement is shown in Fig. 2-3. Table 2-2 lists the results of a number of measurements. These measurements were undertaken in order to verify the high transmission values which were obtained in similar experiments reported on by James (DNA 4238F). In our present set of measurements we have found that our fluorescence signal is smaller than previously observed and we were not able to obtain any signal when a 16 cm cell was placed between the fluorescence cell and the detector, even in the case where this cell was evacuated. Therefore, we constructed a smaller cell which had a path length of 1.5 cm. Even with this cell in place there was considerable attenuation of our fluorescence signal due to having the detector further away from the exit window of the fluorescence cell. We were able to obtain some transmission measurements. The transmission measurements were made by observing the signal with both the fluorescence

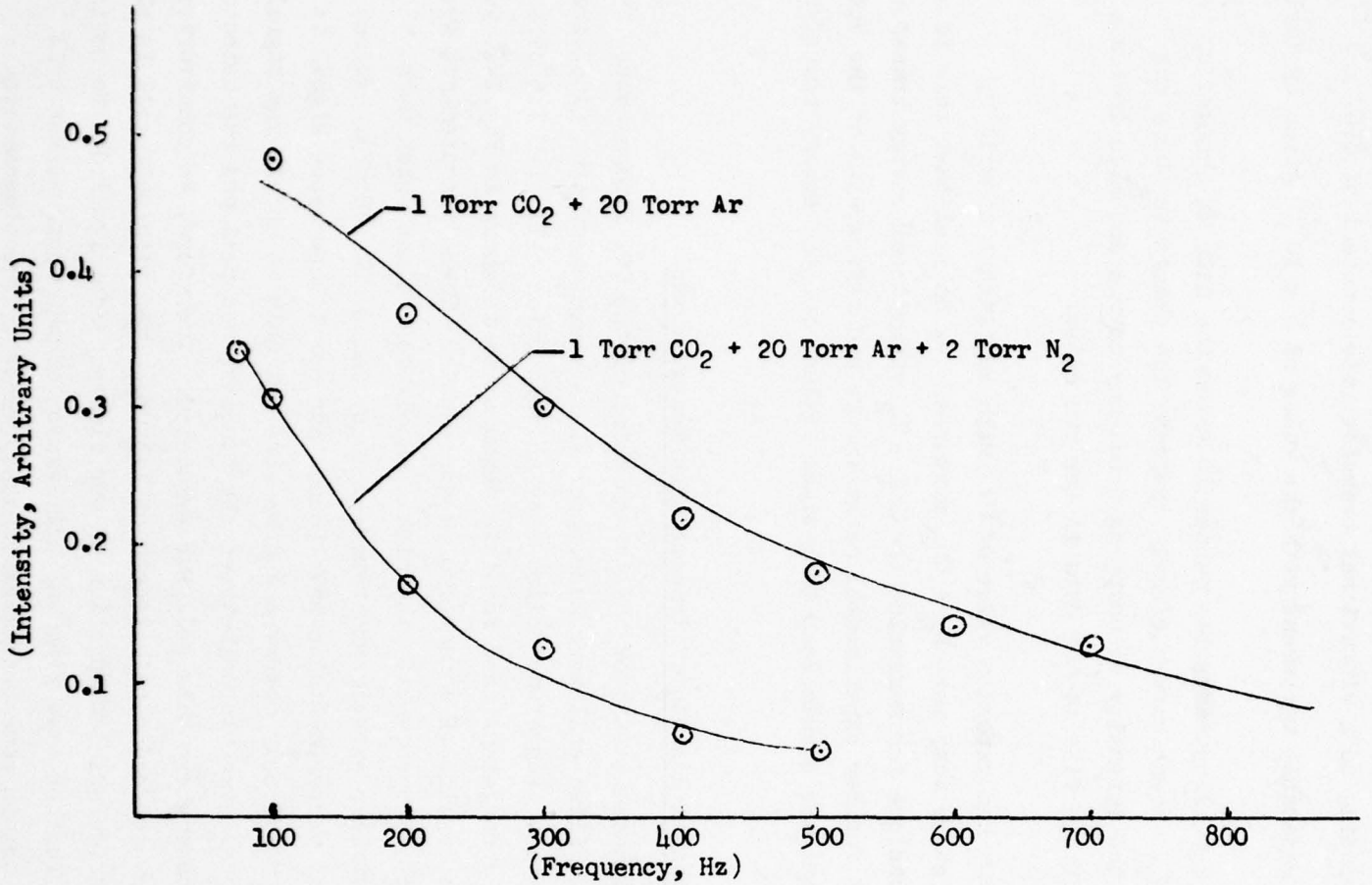

Figure 2-6 Intensity vs Chopping Frequency

Table 2-2

Transmission Measurements

Contents Fluorescence Cell (2 cm path length)	Contents Absorption Cell (1.5 cm path length)	Transmission
1/2 Torr CO_2 + 21 Torr Ar	5 Torr CO_2 + 21 1/2 Torr Ar	(37 ± 8 %)[a]
2 Torr CO_2	2 Torr CO_2	(69 % ± 3 %)[b]
2 Torr CO_2 + 40 Torr He	2 Torr CO_2 + 40 Torr He	63 % ± 8 %
1 Torr CO_2 + 20 Torr He	1 Torr CO_2 + 20 Torr He	71 % ± 8 %
1/2 Torr CO_2 + 20 Torr He	1/2 Torr CO_2 + 20 Torr He	79 % ± 3 %
1 Torr CO_2 + 40 Torr He	5 Torr CO_2	60 % ± 7 %
1 Torr CO_2	1 Torr CO_2	71 % ± 4 %
7.5 Torr CO_2	7.5 Torr CO_2	55 % ± 5 %
1 Torr CO_2 + 40 Torr He	5 Torr CO_2	49 % ± 9 % @ 400 Hz

a) Calculated Value is 22 % for Resonance Band

b) Calculated Value is 38 % for Resonance Band

Transmission measurements were made at a chopping frequency of 100 Hz except where indicated otherwise.

cell and the absorption cell filled with CO_2 and then noting the increase in signal when the absorption cell was evacuated. This measurement could be made without disturbing the position of either cell.

Due to the small signals and large signal to noise associated with some of the measurements in table 2-2 there is a fairly large uncertainty in some of the results. An estimate of this uncertainty is indicated in the table.

The results of these measurements show that the transmissions are still higher than would be expected for from simple considerations for the resonance band and more important hot bands. Our resulting transmission values are not as high as we previously observed in our earlier measurements (James DNA 4238F). The reason for this is not entirely clear. In our present measurements, the geometrical arrangement is different and it may be that the use of a shorter cell in which the possibility of reflection from the walls is greatly diminished has some influence on the results.

As in our earlier measurements, then transmission measurements were made in the hope of being able to obtain information regarding the relative contribution of fluorescent and resonance radiation.
For the first two measurements in the table we have listed a calculated transmission. This transmission was calculated as described in the following paragraphs. The discussion to follow does not take into account multiple scattering effects.

In the event of a gas which is uniformly excited, the observed radiance at the surface should be proportional to the width function $W_b(N\sigma)$ for the band. N represents the number of absorbing molecules in the path length and σ represents the cross section for absorption. Consider two columns of gas with $N\sigma$ values $N\sigma_1$ and $N\sigma_2$ where for our experiment $N\sigma_1$ corresponds to the Fluorescence cell and $N\sigma_2$ corresponds to the absorption cell. In the event that both cells were uniformly excited, the signal would be proportional to $W_b(N\sigma_1 + N\sigma_2)$. This would consist of the signal from cell 1 which is $W(N\sigma_1)$

times the fraction of this transmitted through cell 2 plus the amount of signal $W(N\sigma_2)$ from cell 2. Therefore the transmission can be estimated as

$$T = \frac{W_b(N\sigma_1 + N\sigma_2) - W_b(N\sigma_2)}{W_b(N\sigma_1)} \qquad 2\text{-}12$$

In the event that all of the excitation occurs at the front end of the fluorescence cell, the transmission would be $T_b(N\sigma_1 + N\sigma_2)$ with the absorption cell filled and $T_b(N\sigma_1)$ with the absorption cell empty, thus the observed transmission in this case would be

$$T = \frac{T_b(N\sigma_1 + N\sigma_2)}{T_b(N\sigma_1)} \qquad 2\text{-}13$$

This would represent an upper limit to the transmission.

The first case in table 2-3 has a total $N\sigma_1$ for absorption of the 2.7 μm bands of 6.32 and 7.73 for the 021-000 and 101-000 bands. For these values of $N\sigma_1$ the amount of absorption of 2.7 μm radiation is essentially constant along the length of the fluorescence cell, with the amount ofabsorption in the last .2 cm being about 5 $^{o}/o$ less than in the first 0.2 cm of path.

We show in table 2-3 the results of calculating the band function W_b and T_b for a number of 4.3 μm bands of CO_2. Below the table we show calculated transmission for the resonance bands and hot band 011 → 010 and the fluorescent bands.

The pressures used in the data set of table 2-3 correspond to a voigt profile with a parameter a = 0.9. The band functions were calculated as described in James, DNA 4238F. The parameter a is the ratio $(\sqrt{\ell n\ 2})\gamma_L/\gamma_D$ where γ_L and γ_D are the pressure broadened half width and the Doppler width respectively.

TABLE 2-3

BAND WIDTH AND TRANSMISSION FUNCTIONS
(Voigt Parameter = 0.9)

Band	$W(N\sigma_1)$	$W(N\sigma_2)$	$W(N\sigma_1+N\sigma_2)$	$T(N\sigma_1)$	$T(N\sigma_2)$	$T(N\sigma_1+N\sigma_2)$
626 isotope						
001-000	241.1	684.8	729.32	.201	7.14(-2)	6.71(-2)
021-020	1.215	9.00	10.15	.989	.936	.928
101-100	0.747	5.51	6.23	.993	.960	.954
011-010	42.97	178.8	191.31	.725	.262	.255
636 isotope						
001-000	6.99	45.33	50.24	.949	.712	.685
011-010	0.554	4.19	4.73	.938	.969	.965
628 isotope						
001-000	2.625	18.51	21.81	.980	.873	.858
011-010	0.205	1.53	1.64	.996	.987	.980
627 isotope						
001-000	0.476	3.48	3.99	.994	.974	.970

Fluorescence Cell — Total $N\sigma_1 = 707.4$ (½ Torr CO_2 + 21 Torr Argon, 2 cm path length)

Absorption Cell — Total $N\sigma_2 = 1.061 \times 10^3$ (5 Torr CO_2 + 16½ Torr Argon, 1.5 cm path length)

$$T = \frac{\sum_i W_i(1+2) - W_1(2)}{\sum_i W_i(1)} = 22.7\ \%\ \text{Using all Bands}$$

$$T = \frac{T(N\sigma_1 + N\sigma_2)}{T(N\sigma_1)} = 33\ \%\ \text{for 001 Band}$$

$$T = \frac{\sum_f W_f(1+2) - W_f(2)}{\sum_f W_f(1)} = 95\ \%\ \text{for Fluorescence Bands}$$

The calculated transmission assuming all of the bands contribute is about 22 °/o, which is lower than the observed value. Similar results are shown in table 2-4 for the second case in which 2 Torr of CO_2 are used in both cells. In this case the calculations are made for an a = 0.1 which is quite close to the pure Doppler line shape.

In this second case shown in table 2-5, calculated transmission using equation (2-12) the transmission is 38 °/o. In this case the CO_2 density is greater so that the absorption of 2.7 μm radiation is not completely uniform along the length of the fluorescence cell so that the actual transmission should be greater than this amount, but still less than that calculated from eq. (2-13) which yields a 74 °/o. Our result falls within this range and is expected to be closer to the lower value, so that these results also yield higher than expected transmission based on simple calculations.

These indicate results that we are observing some contributions from the fluorescent transitions 021-020 and 101-100. However, until a detailed calculation is performed which takes into account multiple scattering and possible reflections from the cell walls, we cannot make any positive statements.

We did attempt to make some measurements at reduced temperatures by cooling the fluorescence cell and absorption cell with dry ice. The results obtained were quite uncertain due to interference with subliming dry ice, frosting of the windows and overall decrease in signal due partly to these factors and partly to the changes in the positions of the cells required by the more bulky arrangement required to enclose the cells in a container which could be cooled by addition of dry ice.

Qualitatively it appeared as though cooling led to a few percent increase in the transmission and a decrease in the overall signal. These measurements were only made with pure CO_2 in both the fluorescence cell and the absorption cell. The uncertainty in the measurement was of the same order as the change in transmissions observed. This fact coupled with the

TABLE 2-4

BAND WIDTH AND TRANSMISSION FUNCTIONS
(Voigt Parameter = 0.1)

Band	$W(N\sigma_1)$	$W(N\sigma_2)$	$W(\sigma_1+N\sigma_2)$	$T(N\sigma_1)$	$T(N\sigma_2)$	$T(N\sigma_1+N\sigma_2)$
626 isotope						
001-000	202.8	181.58	253.86	3.05(-2)	3.53(-2)	2.32(-2)
021-020	4.77	3.611	8.098	.922	.941	.869
101-100	2.93	2.21	5.04	.952	.963	.918
011-010						
636 isotope						
001-000	23.11	18.22	35.30	.648	.717	.492
011-010	2.184	1.646	3.77	.964	.973	.938
628 isotope						
001-000	9.745	7.5	16.07	.843	.879	.748
011-010	.816	.610	1.42	.986	.990	.976
627 isotope						
001-000	1.89	1.415	3.249	.968	.976	.949

Fluorescence cell Total $N\sigma_1 = 2.829 \times 10^3$ (2 Torr CO_2, 2 cm path)

Absorption cell Total $N\sigma_2 = 2.122 \times 10^3$ (2 Torr CO_2, 1.5 cm path)

$$T = \frac{\sum_i W_i(1+2) - W_i(2)}{\sum_i W_i} = 43\ \%\text{ using all Bands}$$

$$T = \frac{\sum_f W_f(1+2) - W_f(2)}{\sum_f W_f(1)} = 95\ \%\text{ for Fluorescent Bands}$$

$$T = \frac{T(N\sigma_1 + N\sigma_2)}{T(N\sigma_1)} = 76\ \%\text{ for 001 Band.}$$

This fact that the temperature of the cells could not be accurately measured led us to abandon these measurements. Qualitatively the overall decrease in signal suggests that hot bands contribute to the result, whereas the transmission measurements were of no use in this regard.

Our measurements in the previous section in which we studied intensity as a function of chopping frequency can be interpreted to suggest that fluorescent transitions play no significant part in the observed 4.3 μm signal. This is described in the following section.

2.6 Frequency Dependence of Combined Fluorescence and Resonance Transitions

In this section, we consider briefly the case in which we have fluorescent bands such as 021 - 020 and resonance bands 001 → 000 contributing and in which the fluorescent state 021 is produced by sinusoidial excitation and the resonant state is produced by energy transfer between 021 and ground state molecules.For simplicity we consider just one resonance band and one fluorescence band, although the results can be generalized to apply to any number of such bands.

The rate of formation of the 021 level is given by

$$\frac{d(021)}{dt} = e^{iwt} - k_1(021)(000) \qquad (2\text{-}14)$$

The rate of formation of 001 is given by

$$\frac{d(001)}{dt} = k_1(021)(000) - k_2(001)(M) \qquad (2\text{-}15)$$

where k_1 is the rate constant for

$$(021) + (000) \overset{k_1}{\rightleftarrows} (020) + (001) \qquad (2\text{-}16)$$

and $k_2(M)$ is the rate at which (001) is quenched.

Writing $k_2(M) = k$ and $\tau = \frac{1}{k_1(000)}$ where τ is a time constant for the transfer reaction (2-16), the resulting intensity which is in phase with the excitation source is proportional to

$$\text{Intensity} \propto \frac{A\tau}{1 + \omega^2\tau^2} + \left[\frac{k - \omega^2\tau}{(1 + \omega^2\tau^2)(k^2 + \omega^2}\right] \qquad (2\text{-}17)$$

The first term in this expression is the contribution from the fluorescence and the second term is the contribution due to the resonance bands. From this expression it is clear that as $\tau \rightarrow 0$, corresponding to an extremely rapid transfer reaction (2-16), the results reduce to the simple Lorentizian shape used in section 2-4 of this report.

The factor A is inserted in equation 2-17 to account for the difference in transmission of the resonance and fluorescence bands. In attempts to fit our data to equation 2-17 we found that the data was still fit by a Lorentzian. For small values of τ such that $\omega\tau < 1$, the fluorescence term is essentially a constant $A\tau$. In various fits of the data the constant term $A\tau$ was found to be small and variable from one set of data to another, sometimes being positive or negative. We conclude from this that the fluorescent bands are not contributing significantly to the observed 4.3 μm emission.

2.7 Advantages of Using a Laser Source Rather Than a Blackbody

In this section we discuss the reasons why we believe that a laser source is necessary in order to study the direct fluorescence from the levels 021 and 101 which are excited by 2.7 μm radiation.

2.7.1 Limitation on Results Using a Blackbody Source

In our experiments to measure fluorescence at 4.3 μm we have used an infrared industries blackbody source followed by a narrow bandpass filter at

2.7 μm in order to excite the 101 and 021 levels of CO_2. A 4.3 μm filter placed in front of the detector enables us to measure 4.3 μm fluorescence produced on irradiating CO_2 at 2.7 μm. By placing a cell filled with CO_2 between the fluorescence cell and the detector we measure the attenuation of the 4.3 μm radiation which is absorbed by CO_2. In this manner we hoped to distinguish between the direct decay of the levels 021 and 101 to 020 and 100 respectively (which would produce 4.3 μm emission which is not absorbed by ground state CO_2) and 4.3 μm emission due to decay of the 001 levels which can be produced in energy transfer collision of the type

$$\begin{matrix}101\\021\end{matrix} + CO_2(000) \xrightarrow{k} \begin{matrix}100\\020\end{matrix} + CO_2(001)$$

The analysis of this data is complicated by the fact that a large number of isotope bands and hot bands near 4.3 μm can also be excited. By going to sufficiently low partial pressures of CO_2 it should be possible to produce a situation where the direct decay of 101 and 021 by emission at 4.3 μm is the most important radiative process at 4.3 μm. The lowest feasible CO_2 concentrations are limited by the intensity of the blackbody source and the sensitivity of the detector. In our experiments to date the lowest pressure utilized has been of the order 1 Torr. Comparing the radiative lifetime for 4.3 μm emission with the energy transfer rate $k(CO_2)$ for intramolecular VV transfer via

$$\begin{matrix}021\\101\end{matrix} + (000) \rightarrow \begin{matrix}020\\100\end{matrix} + (001),$$

these will be equal when

$$k(CO_2) = 440 \text{ sec}^{-1}$$

Thus at partial pressures of the order of 1 Torr = 3.26×10^{16}, radiation and energy transfer will be equally likely for values of k of the order of 10^{-14} cm^3 sec^{-1}. The measurements of Finzi and Moore (1975) suggest that the rate constant for the VV transfer reaction (4) is of the order of 10^{-10}. Thus in order to study the fluorescence under conditions where reaction (4) is not important, it is necessary to work at much lower pressures than we have

utilized. At pressures of the order of a few microns, the amount of 2.7 μm absorption in a small cell is inadequate to produce a measureable signal with our Blackbody light source.

This limitation can be overcome by using a laser as a light source which due to the large number of incident photons will result in a much greater number of molecules excited to the levels 101 and 021.

2.7.2 Characteristics of Tunable Infrared Laser

In this section we describe the characteristics of the tunable infrared laser and discuss the increase in signal-to-noise which we can expect to achieve using this source.

The Infrared Laser system consists of a tunable dye laser and an optical parametric oscillator (OPO) utilizing a Lithium Niobate crystal as a non-linear element. The high intensity visible light from the dye laser is converted into infrared radiation by the OPO. Tuning in the infrared is achieved by tuning the dye laser.

The infrared output consists of a series of modes lying within about a 0.5 cm^{-1} envelope. Each individual mode has a width of the order of 0.001 cm^{-1} and the mode spacing is of the order of 0.025 cm^{-1}. The laser can be made to produce an infrared output out to about 2.85 μm. The total energy in a single pulse is of the order of 5×10^{-5} joules with a pulse duration of the order of 1 microsecond. In our application it is necessary to tune the system so that a single mode is centered on the absorption line of interest. The energy in the more intense single modes is of the order of 1/20th of the total energy in the pulse.

In order to estimate the improvement we can expect using a laser source we make a comparison between the amount of energy absorbed from a 2.7 μm beam by CO_2 and the NEP of the InSb detector with the corresponding quantities for a laser pulse. An estimate of the amount of the number of photons absorbed in experiments using a blackbody source can be obtained from the discussion given in the report DNA 4238F by James.

The amount of absorption in the 021 band of CO_2 can be estimated following the discussion in section VI of DNA 4238F. At a pressure of one Torr the total excitation rate in this band is approximately 2.5×10^{-6} watts/cm^3, which corresponds to ~ 3.3 c 10^{13} photon/sec-cm^3 of 2.7 μm radiation absorbed. The NEP of the InSb detector is approximately 10^{-12} watts/$\sqrt{Hz}$ or (2.15×10^7 photons/sec - $\sqrt{Hz}$). The output of a single mode near 2.7 μm from the infrared laser contains approximately 3.4×10^{13} photons in a single mode. The absorption per cm of path at line center for a Doppler Shaped Line is given by

$$k(v_o) = \frac{4.16 \times 10^{-13}}{\gamma_D} XNf$$

where N is the total number of molecules, X in the fraction of molecules in the absorbing level, f is the oscillator strength of the transition and γ_D is the Doppler width in cm^{-1}. When the appropriate numbers for the most intense line of the 021-000 band are inserted into this expression, the resulting line center absorption is .32/cm. The resulting absorption per cm^3 is approximately 10^{13} photons/cc at 1 Torr CO_2 partial pressure.

The laser pulse is of the order of 1 microsecond in duration, however, the actual decay of fluorescence will be different from this depending on the pressures used, quenching rates, etc. Some estimate of the quenching lifetimes is given by the following expression:

$$\tau \sim \frac{1}{k(m)}$$

At one Torr $m = 3.2 \times 10^{16}$ and for $k \sim 10^{-10}$ the resulting lifetime is approximately .3 μsec. Since the laser pulse is 1 μsec in duration, such a small decay constant would be difficult to measure. In the event that k in Eq. (1) is of the order of 10^{-10}, then partial pressures of CO_2 in the range .01 Torr would yield decay times of the order of 30 μsec. If one considers the measurement of a pulse in a 30 μsec time interval, the effective bandwidth is of the order of $1/30 \times 10^{-6} \sim 3.3 \times 10^4$ Hz, so that the detector N.E.P becomes

$$\text{NEP} \cong (10^{-12} \text{ watts}/\sqrt{\text{Hz}}) \; (\sqrt{3.3 \times 10^{4} \text{ Hz}}$$

$$\cong 1.82 \times 10^{-10} \text{ watts}$$

$$\cong 3.9 \times 10^{9} \text{ photons/sec.}$$

In a time interval of 30 μsec, this corresponds to a noise level of 1.17×10^{5} photons. In order to achieve this 30 μsec time constant, only $1/100 \times 10^{13}$ or $\sim 10^{11}$ photons are absorbed per cm^3. The relative increase in signal-to-noise for the laser compared with the blackbody source is proportional to the ratio

$$\left(\frac{\text{Excitation rate}}{\text{NEP}} \right)_{\text{Laser}} \Bigg/ \left(\frac{(\text{Excitation Rate})}{(\text{NEP})} \right)_{\text{Blackbody}}$$

These should be compared at the same pressures. Therefore, the Blackbody excitation rate should be decreased to 3.3×10^{11}. Comparing the above ratio gives

$$\left(\frac{10^{11}}{1.17 \times 10^{5}} \right) \Bigg/ \frac{(3.3 \times 10^{11})}{2.15 \times 10^{7}} \cong 56$$

The laser we are considering using has a pulse rate of up to 30 pps. so that the data gathered in a second will have a signal/noise of about $\sqrt{30}$ times greater. Thus the laser can be expected to be about a factor of 300 better than the blackbody source in so far as signal-to-noise is concerned.

In order that we are able to take advantage of the signal/noise capability of the pulsed laser source, we need an instrument capable of collecting the signals over a short time interval and averaging the results of repetitive pulses. For this purpose we have available a PAR model 160 Boxcar Integrator which has a resolution capability of 10 nanosec. This time resolution is variable and can be selected to match the pulse duration in a particular experiment. With this instrument we can measure the total signal contained in

a fluorescent decay curve, or by selecting the time interval we can look at various portions of the decay curve and in this manner measure the actual decay curve. We also have available a Northern Scientific Model 540 digital signal averager with 10 μsec time resolution. This instrument samples 10 μsec segments of a single pulse so that a decay curve can be obtained by repetitive averaging of the measured pulses. A lower limit to the decay times that could be measured with this instrument would be of the order of a hundred μsec which would correspond to 10 samples of the curve in each pulse.

Earlier in this section we mentioned the fact that the laser could be tuned to align a particular mode with the center of an absorption. The chromatix laser system which we are planning for these studies can be coarse tuned so that the absorption line is within the envelope containing the output modes from the OPO. Additional fine tuning may be required to place a single mode at line center. This can be done by means of a piezoelectric crystal driven by a ramp voltage supply which is attached to one of the mirrors in the dye laser. By this means, the cavity dimension can be changed slightly so as to scan over a free spectral range ($0.025\ cm^{-1}$) which will enable a single mode to be positioned on the line center. This is not included with the chromatix laser, but they have plans available from which such a fine tuning device can be constructed.

The output beam from the OPO is of the order of 1 mm diameter. For our experiment we plan to expand the beam to the order of 1 cm diameter by constructing a beam expander utilizing two lenses of suitable focal length.

2.7.3 Advantages of Laser for Studying the 2.7 → 4.3 μm Fluorescence Mechanism

Due to the increased sensitivity obtainable with the laser source as described in the previous section, it is possible to make measurements at short time intervals following the excitation pulse. Measurements of the signal at 2.7 μm and at 4.3 μm should correspond to the emission from the same upper level so that the relative signals immediately following excitation pulse should provide a Measurement of the Branching ratio for emission of 4.3 μm

and 2.7 μm radiation. At longer times the 2.7 μm radiation may be completely quenched by the intramolecular VV transfer reaction. The 4.3 μm signal will still persist, however, so that in order to measure the Branching ratio it is essential that measurements be extrapolated to very early times following the excitation. In the case of the excitation with a blackbody source, this is not possible. The relative Branching ratios using such a source could only be obtained by going to conditions where molecular collisions and wall collisions are not affecting the results. The lack of sensitivity utilizing a blackbody source makes such a measurement exceedingly difficult if the rate constant k for the intramolecular VV transfer reaction is really of the order $k \cong 10^{-10}$.

In order to measure the 2.7 μm Fluorescence it may be desirable and/or necessary to have a filter which will transmit only one branch of the 2.7 μm bands, and tune the laser to excite a line in the other branch so that the detector is not adversely affected by a large pulse of scattered light from the laser excitation pulse.

2.8 References

2-1 Finzi, J., and C. B. Moore, J. Chem. Phys., 63, 2785, 1975

2-2 James, T. C., "Laboratory Study of Infrared Fluorescence of CO_2," DNA 4238F, HAES Report No. 60, Dec. 1976

2-3 Rosser, W. A. Jr., and E. T. Gerry, J. Chem. Phys, 51, 2286, 1969

2-4 Stephenson, J. C., R. E. Wood and C. B. Moore, J. Chem. Phys., 54, 3097, 1971

2-5 Taylor, R. L., Can. J. Chem., 52, 1436, 1974

3.0 THE CO_2 4.3 μm ZENITH SPECTRAL RADIANCE MODEL

3.1 Introduction

In this section we describe a numerical facility that we have developed to calculate CO_2 4.3 μm zenith spectral radiance in order to model the spectral structure in the CO_2 4.3 μm zenith spectral radiance data which have been obtained in three events in the DNA/AFGL auroral measurements program. These three include data obtained by the 1 April 1976 HIRIS flight into moderate auroral activity and short wavelength CVF spectrometer data that were obtained in undisturbed night time conditions (11 April 1974) and under extremely active auroral breakup conditions (24 March 1973). We present the results of the modeling effort and discuss the relevant implications with regard to the auroral and nuclear infrared background problem.

3.2 Details of the Calculation

To accurately model the spectral structure in the zenith radiance component near 4.3 μm which results from CO_2 emission requires that we compute the radiance R_{jkb} in each of 2420 lines in the CO_2 4.3 μm complex. The quantity R_{jkb} is the radiance in a line in the band designated by j, k is the rotational quantum number of the ground state and b is the branch (the p and r branches are dominant for the 4.3 μm bands). The bands that are included in the calculation are shown in Table 3.1. In previous publications Kumer (References 3-1 and 3-2) has shown that these bands form a complete set for the calculation of atmospheric CO_2 non-LTE 4.3 μm radiance formed above 50 km altitude.

The calculation of the R_{jkb} for a given altitude z first requires that we solve the time dependent plane parallel radiative transport equations as is described in references 3-1 and 3-2 in order to obtain $\Omega_j(N_j)\ S_j(N_j)$ the 4.3 μm volume emission in band j at altitude z. The notation that we use in our discussion has for the most part been defined in references 3-1 through 3-4. In this report we will occasionally redefine some of the more critical notation in order to facilitate readability. For example, $N_j = \int_z dz'[CO_2]G_j$ is the

Table 3.1

THE CO_2 ν_3 BANDS

j	$CO_2(j\nu_3) \rightarrow (j)$ Transition	Isotope*
1	$00^0 1 \rightarrow 00^0 0$	626
2	$00^0 1 \rightarrow 00^0 0$	636
3	$00^0 1 \rightarrow 00^0 0$	628
4	$00^0 1 \rightarrow 00^0 0$	627
5	$01^1 1 \rightarrow 01^1 0$	626
6	$01^1 1 \rightarrow 01^1 0$	636
7	$01^1 1 \rightarrow 01^1 0$	628
8	$01^1 1 \rightarrow 01^1 0$	627
9	$02^2 1 \rightarrow 02^2 0$	626
10	$02^0 1 \rightarrow 02^0 0$	626
11	$10^0 1 \rightarrow 10^0 0$	626

* The notation 626 designates the $^{16}O^{12}C^{16}O$ isotope, etc.

column density above altitude z of the band j CO_2 ground state specie. The R_{jkb} are then calculated via an integral of the product of volume emission in a given line jkb weighted by the transmission for that line between emission point z′ and the position z of the rocket borne sensor. The integral must be computed for each of the lines jkb. The integral is

$$4\pi R_{jkb}^{(z)} = \int_o^{N_j(z)} d\tau'_{jkb}\, T(\tau'_{jkb})\, \Omega_j(N'_j)\, S_j(N'_j) \quad .$$

Here x_k is the fractional population of the kth rotational state, $\tau_{jkb} \cong s_{jkb}\, x_k (N_j(z) - N_j(z'))\sigma$ is the optical depth at line center between altitude z and z′ for the line jkb, and $T(\tau) \equiv \int dx / \sqrt{\pi}\, \varphi(x)\, e^{-\tau\varphi(x)}$ is the single line transmission function, $\varphi(x)$ is the Voigt profile. We use a Lorentz parameter 10^{-3} in the calculation of $\varphi(x)$, this selection is discussed in reference 3-3. The s_{jkb} may be calculated from the Hönl-London formulas which are conveniently listed in reference 3-5.

In order to calculate the spectral structure as a function of altitude in 4.3 μm zenith spectral radiance data, it is necessary to calculate the array of the line radiances R_{jkb} for each altitude mesh point of interest. Each line is centered at wavelength λ_{jkb}. These wavelengths are available in a tabulation on a computer tape which has been provided to LMSC by AFGL. The tabulation is discussed in reference 3-6.

To model the observed spectral radiance $R(\lambda)$ we use the spectral response $F(\lambda,\lambda')$ for the instrument which was used to obtain the data to compute synthetic spectra via

$$R(\lambda) = \sum_{jkb} R_{jkb}\, F(\lambda, \lambda_{jkb}) \quad .$$

The sum is taken over the entire array of line brightnesses.

A block diagram illustrating the flow of the CO_2 4.3 μm zenith spectral radiance calculation is shown on Figure 3-1. The fractional population f_j of the j band upper state CO_2 specie and the column density N_j of the ground state

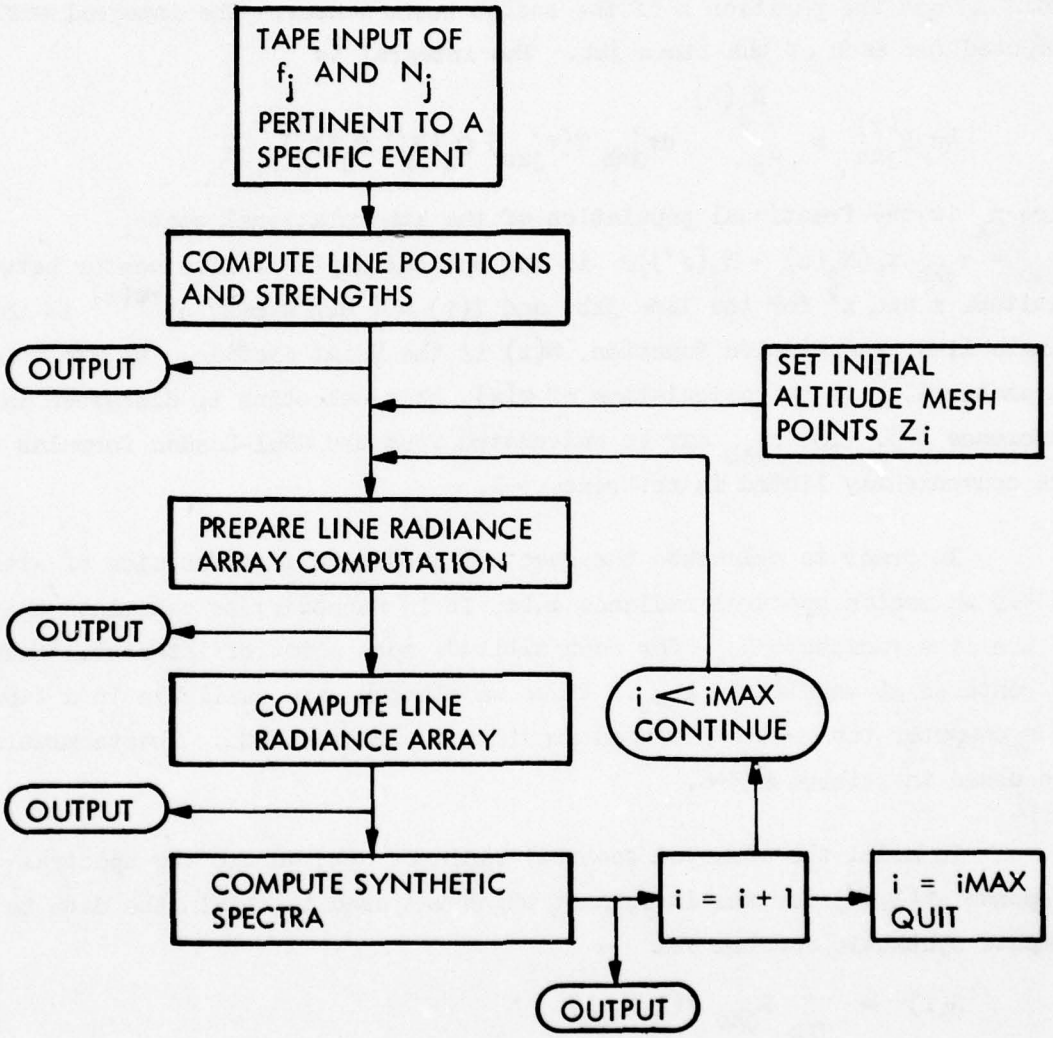

Figure 3-1. A schematic of our model for predicting CO_2 4.3 μm spectral zenith radiance.

specie were precalculated for each of the events under consideration by methods described in references 3-1 and 3-2, and stored on tape. Tape read input of f_j, N_j and parameters related to the atmospheric model and to the spectroscopy and radiation transport of CO_2 initiate the calculation.

3.3 Results

Data Obtained 11 April 1974:

Here we discuss the comparison of our CO_2 4.3 μm spectral radiance calculation with data obtained 11 April 1974 under non auroral night time conditions via a rocket borne liquid N_2 cooled CVF spectrometer as described by Wheeler et al. (reference 3-7).

The final published version of the spectrally integrated zenith radiance data for this event are represented by the solid curve labeled D on Figure 3-2. This curve differs slightly from the preliminary version of these data which have been previously evaluated by Kumer (reference 3-1), but the difference is not enough to make any change whatever in the qualitative evaluation of these data as given by Kumer (reference 3-1). In particular, satisfactory interpretation of these data may be achieved by utilizing the $OH(V) \overset{VV}{\rightarrow} N_2 \overset{VV}{\rightarrow} CO_2(\nu_3) \rightarrow CO_2 + h\nu_{4.3\ \mu m}$ mechanism which was originally presented by Kumer (reference 3-1). The final version of the 11 April 1974 data require that about 0.14 ergs/cm^2 sec of vibrational energy is transferred from OH(V) to N_2. A slightly different model kinetic temperature is also required to achieve the quality of fit as shown on Figure 3-2. Details of this final evaluation of the final version of the 11 April 1974 data are given in a paper by Kumer et al. (reference 3-8).

Samples of the results of using our spectral modeling facility in application to selected 11 April 1974 CVF spectral scans which are published in reference 3-7 are shown on Figures 3-3. The appropriate CVF slit function $F(\lambda, \lambda')$ was obtained from Tom Condron (reference 3-9) of AFGL and the appropriate resolution element for the CVF which was used on 11 April 1974 is given in reference 3-7. For the 11 April 1974 SWIR CVF the slit function $F(\lambda, \lambda')$

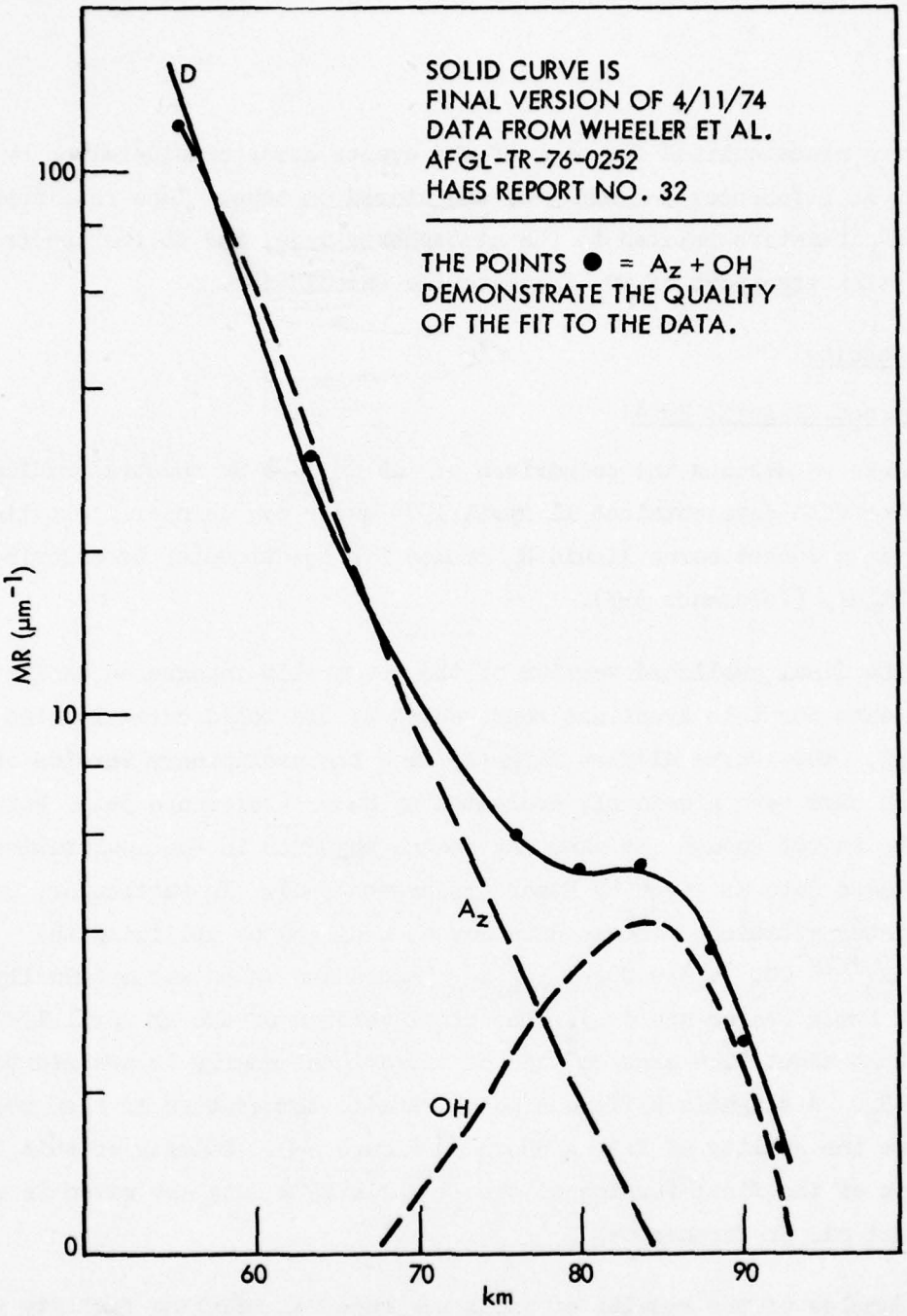

Fig. 3-2. The solid curve labeled D represents the final version (Ref.3-8) of the 4.3 μm peak spectral zenith radiance data which were obtained 11 April 1974. Curve A_z is a non-LTE radiation transport computation of the 4.3 μm peak spectral radiance that would be produced by the two mechanisms (i) thermal collusions and (ii) absorption of earthshine. The curve OH is a computation of the 4.3 μm peak spectral radiance due to the $OH(V) \xrightarrow{VV} N_2$ mechanism. A vibration transfer of 0.14 ergs/cm^2 sec from OH(V) to N_2 is required to obtain the high quality fit to the data A_z+OH which are illustrated by the points ●.

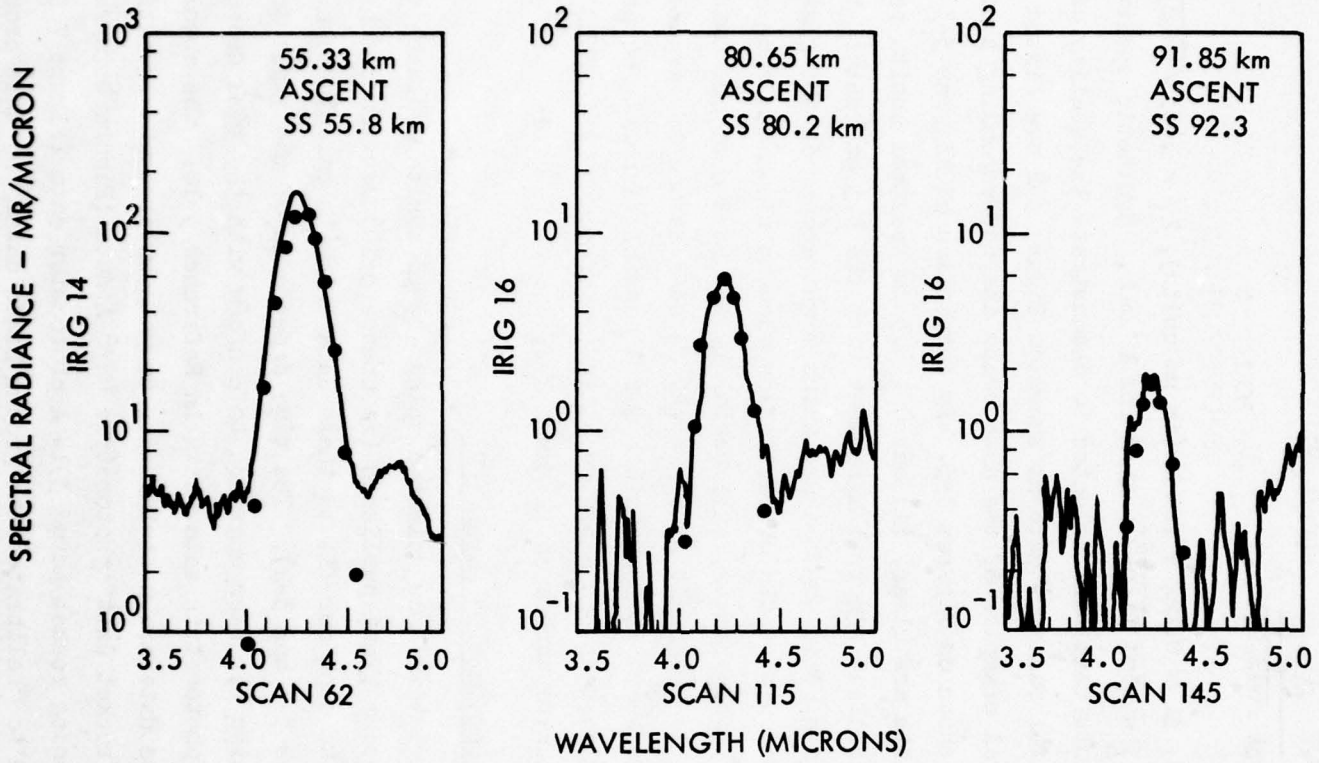

Figure 3-3. The points • on Figures 3-3 represent our synthetic spectra calculated at a 0.05 μm interval. The synthetic spectra are compared with data scans for 11 April 1974 that were reported in Reference 3-7. The altitude for which the synthetic spectra were calculated are labelled by the prefix SS on the figures.

may be approximated by

$$F(\lambda,\lambda') \quad \frac{2}{\Delta\lambda\sqrt{\pi\ln(2)}} \quad e^{-(\lambda w/\lambda_i)^2}$$

where $\lambda w = (\lambda' - \lambda)$, $\Delta\lambda \cong 0.122 + .01\lambda$ (in μm units), $\lambda_i = .433\sqrt{\ln(2)}\,\Delta\lambda/2$ for $\lambda' < \lambda$ and $\lambda_i = \lambda_L = .567\sqrt{(\ln(2)}\,\Delta\lambda/2$ for $\lambda' > \lambda$. Synthetic spectra for the altitude mesh points that were selected to demonstrate the quality of the fit to the peak spectral radiance data as shown on Figure 3-2 are listed in Table 3.2. Several examples of the data scans and corresponding synthetic spectra are also shown on Figures 3-3. By inspection of Figures 3-3 and Table 3.2 two points are clear, (i) our CO_2 4.3 μm spectral zenith radiance model provides excellent spectral agreement with the 4.3 μm feature that is apparent in the data, (ii) any feature which might appear in the region $\lambda \geq 4.5$ μm in data obtained with a CVF of resolution element width the same as the 11 April 1974 CVF, or narrower, will certainly not be due to CO_2 emission. This second point is important since it may be used as another argument that CO_2 is not the emitter which is responsible for a possible auroral feature in the 4.5 to 4.6 μm region that was noted by Stair (reference 3-9) in SWIR CVF data obtained in a moderate aurora on 12 March 1975.

Results for Data Obtained 24 March 1973

On Figure 3-4 we show selected upleg 4.3 μm zenith radiance data points taken from the recent final published (reference 3-10) version of the 24 March 1973 data. We also show our fit to these data which is calculated by the TDT method (references 3-1 and 3-2). The time dependence of the input model we use for this calculation has been upgraded to conform with the time dependence of the ground based photometric data shown in Reference 3-10. The absolute magnitude of these data are uncertain due to unknown atmospheric extinction. The ground based "rocket exit" photometric 4278 Å data (Figure 4 in reference 3-10) and the downleg rocket borne 3914 Å photometer data (Figure 7 in reference 3-10) may be used to "calibrate" the ground based data. By this procedure we infer that the maximum 3914 Å brightness, which occurred some time like 50 to 150 sec after launch, was about 420 kR. The quality of our fit to the final

Table 3.2

SYNTHETIC SPECTRA FOR 11 APRIL 1974 AT SELECTED ALTITUDES.
THE COMPUTER GENERATED NUMBERS ARE IN STANDARD FLOATING POINT FORMAT.

	SPECTRAL BRIGHTNESS IN MR/μm							
λ (μm)	92.3 km	90.2	88.1	83.8	80.2	76.1	63.8	55.8
.3900+01	.1935-03	.3082-03	.4723-03	.7271-03	.7367-03	.7726-03	.2657-02	.9058-02
.3950+01	.2224-02	.3514-02	.5341-02	.8016-02	.7945-02	.8263-02	.2924-01	.1002+00
.4000+01	.1717-01	.2692-01	.4060-01	.5950-01	.5780-01	.5984-01	.2192+00	.7588+00
.4050+01	.9002-01	.1401+00	.2099+00	.3011+00	.2875+00	.2976+00	.1136+01	.3990+01
.4100+01	.3246+00	.5022+00	.7479+00	.1054+01	.9928+00	.1033+01	.4131+01	.1480+02
.4150+01	.8153+00	.1255+01	.1861+01	.2587+01	.2421+01	.2550+01	.1072+02	.3936+02
.4200+01	.1445+01	.2218+01	.3280+01	.4533+01	.4247+01	.4562+01	.2023+02	.7648+02
.4250+01	.1806+01	.2769+01	.4093+01	.5668+01	.5371+01	.5942+01	.2801+02	.1097+03
.4300+01	.1499+01	.2306+01	.3425+01	.4844+01	.4754+01	.5530+01	.2806+02	.1151+03
.4350+01	.7907+00	.1232+01	.1860+01	.2796+01	.2961+01	.3720+01	.2054+02	.8891+02
.4400+01	.2580+00	.4123+00	.6424+00	.1084+01	.1303+01	.1837+01	.1132+02	.5189+02
.4450+01	.5264-01	.8785-01	.1453+00	.2964+00	.4253+00	.6947+00	.4873+01	.2351+02
.4500+01	.7103-02	.1280-01	.2353-01	.6245-01	.1078+00	.2011+00	.1580+01	.8001+01
.4550+01	.7242-03	.1461-02	.3088-02	.1049-01	.2058-01	.4178-01	.3549+00	.1890+01
.4600+01	.6310-04	.1409-03	.3311-03	.1297-02	.2706-02	.5744-02	.5146-01	.2891+00

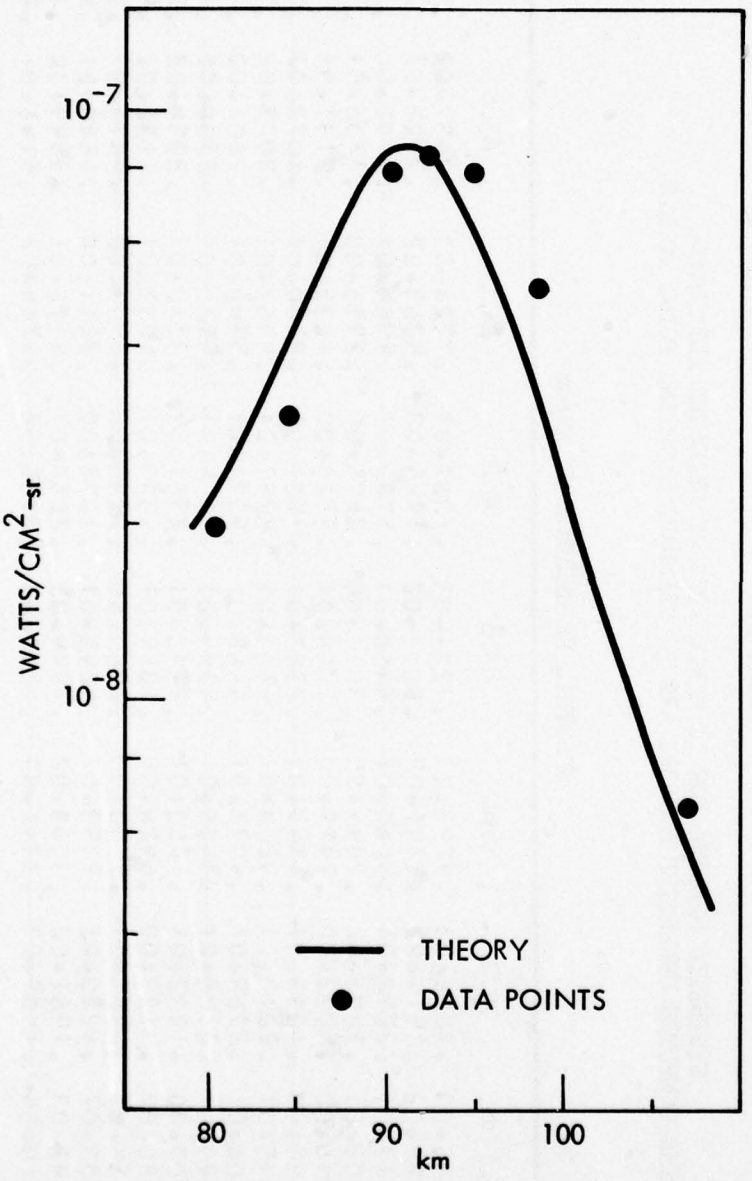

Figure 3-4. Our upgraded TDT model calculation (the solid curve) for the 24 March 1973 upleg CO_2 4.3 μm zenith radiance profile is compared with selected data points for the final version of these data which were published by reference 3-12.

version of the 24 March 1973 upleg 4.3 μm zenith radiance data which is shown on Figure 3-4 is as good or better than we had achieved in our earlier evaluation (references 3-1, 3-2 and 3-3) of the preliminary version of these data. A value $\epsilon \simeq 10.4$ N_2^+ produced per ionization event is required to fit the data as shown.

In order to model the 24 March 1973 upleg zenith 4.3 μm spectral radiance data we used a SWIR CVF spectrometer slit function $F(\lambda, \lambda')$ that was essentially identical to that which we used to model the 11 April 1974 data. Information on the 24 March 1973 slit function was provided by reference 3-11. The synthetic spectrum we calculate in this way is compared with a 24 March 1973 86 km upleg SWIR CVF spectrometer data scan (preliminary data, reference 3-12) on Figure 3-5. The synthetic spectrum appears slightly broader than the data and slightly blue shifted. The overall blue shift is probably a result of the way the wavelength scale was assigned to the preliminary data reported in reference 3-12. The relative broadening of the synthetic scan versus the data suggests that the CVF achieved somewhat better resolution than nominal. Synthetic auroral spectra for the 24 March 1973 upleg are listed in Table 3.3.

On Figure 3-6 we show a comparison of the 24 March 1973 86 km upleg data scan with a 2cd synthetic spectrum that is calculated by the use of a resolution element $\Delta\lambda = 0.9 \times (0.122 + .01\,\lambda)$ that is about 10% narrower than the nominal value. Better agreement with respect to the width of the 4.3 μm data feature is attained in this 2cd case as was expected.

Results for Data Obtained 1 April 1976

On 1 April 1976 the HIRIS was launched into a moderate aurora. Spectral zenith radiance data with about 2 cm^{-1} resolution were obtained in the 4.3 μm region.

A preliminary prediction for auroral and ambient components of the 4.3 μm zenith radiance is plotted as a function of altitude on Figure 3-7. The ambient component is calculated on the basis of a March 65° N model atmosphere

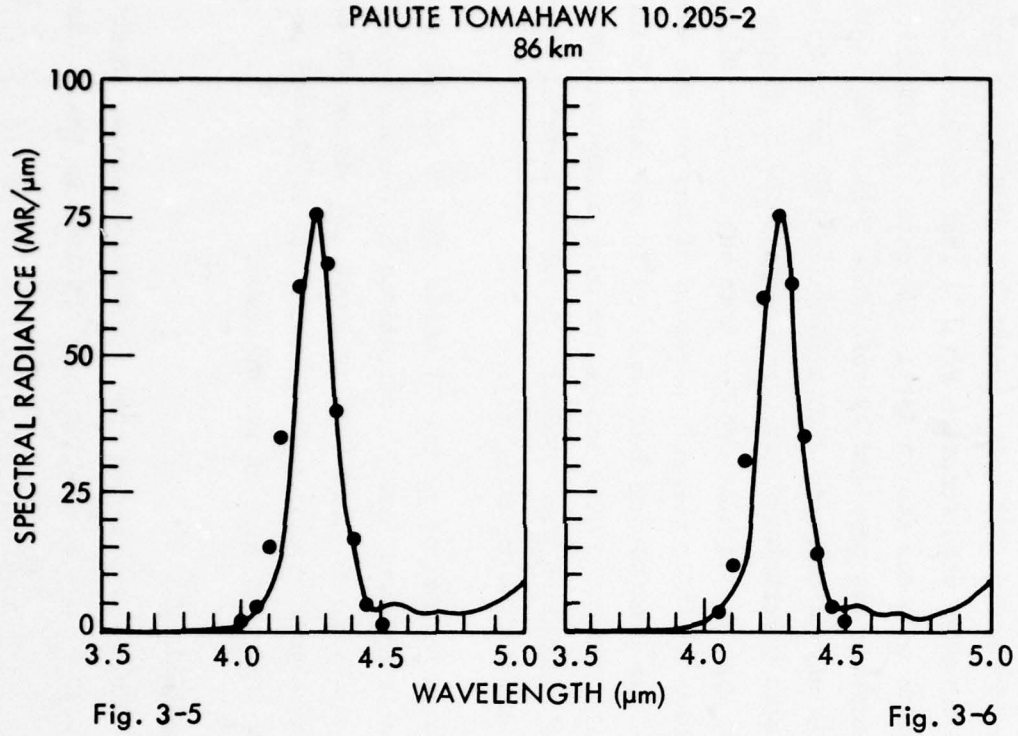

Figs. 3-5 and 3-6. The plotted points are our predicted synthetic spectra for the 24 March 1973 upleg. These are compared with a published (reference 3-12) preliminary data scan (the solid curve) obtained at 86 km altitude in Figure 3-5 and 3-6. The resolution element $\Delta\lambda = 0.9 \times \Delta\lambda$ was used in computing the points shown on Figure 3-6.

Table 3.3.

SYNTHETIC SPECTRA FOR 24 MARCH 1973 UPLEG AT SELECTED ALTITUDES.

	SPECTRAL BRIGHTNESS IN MR/μm						
λ (μm)	107.1 km	98.6	94.9	92.4	88.1	83.7	80.2
.3900+01	.7115-03	.4307-02	.9765-02	.1352-01	.1416-01	.9576-02	.5577-02
.3950+01	.8372-02	.5020-01	.1125+00	.1549+00	.1561+00	.1025+00	.5826-01
.4000+01	.6599-01	.3922+00	.8700+00	.1178+01	.1161+01	.7389+00	.4101+00
.4050+01	.3522+00	.2077+01	.4565+01	.6121+01	.5884+01	.3631+01	.1973+01
.4100+01	.1287+01	.7544+01	.1645+02	.2187+02	.2057+02	.1236+02	.6593+01
.4150+01	.3259+01	.1902+02	.4123+02	.5447+02	.5034+02	.2962+02	.1562+02
.4200+01	.5785+01	.3369+02	.7279+02	.9581+02	.8765+02	.5099+02	.2683+02
.4250+01	.7198+01	.4192+02	.9049+02	.1190+03	.1085+03	.6307+02	.3353+02
.4300+01	.5865+01	.3434+02	.7450+02	.9841+02	.9097+02	.5432+02	.3003+02
.4350+01	.2956+01	.1761+02	.3888+02	.5230+02	.5085+02	.3288+02	.1983+02
.4400+01	.9042+00	.5566+01	.1267+02	.1761+02	.1872+02	.1390+02	.9635+01
.4450+01	.1713+00	.1124+01	.2683+01	.3912+01	.4743+01	.4265+01	.3506+01
.4500+01	.2175-01	.1619+00	.4136+00	.6409+00	.9103+00	.1004+01	.9633+00
.4550+01	.2194-02	.1966-01	.5354-01	.8782-01	.1417+00	.1806+00	.1906+00
.4600+01	.1986-03	.2056-02	.5803-02	.9784-02	.1678-01	.2287-01	.2523-01

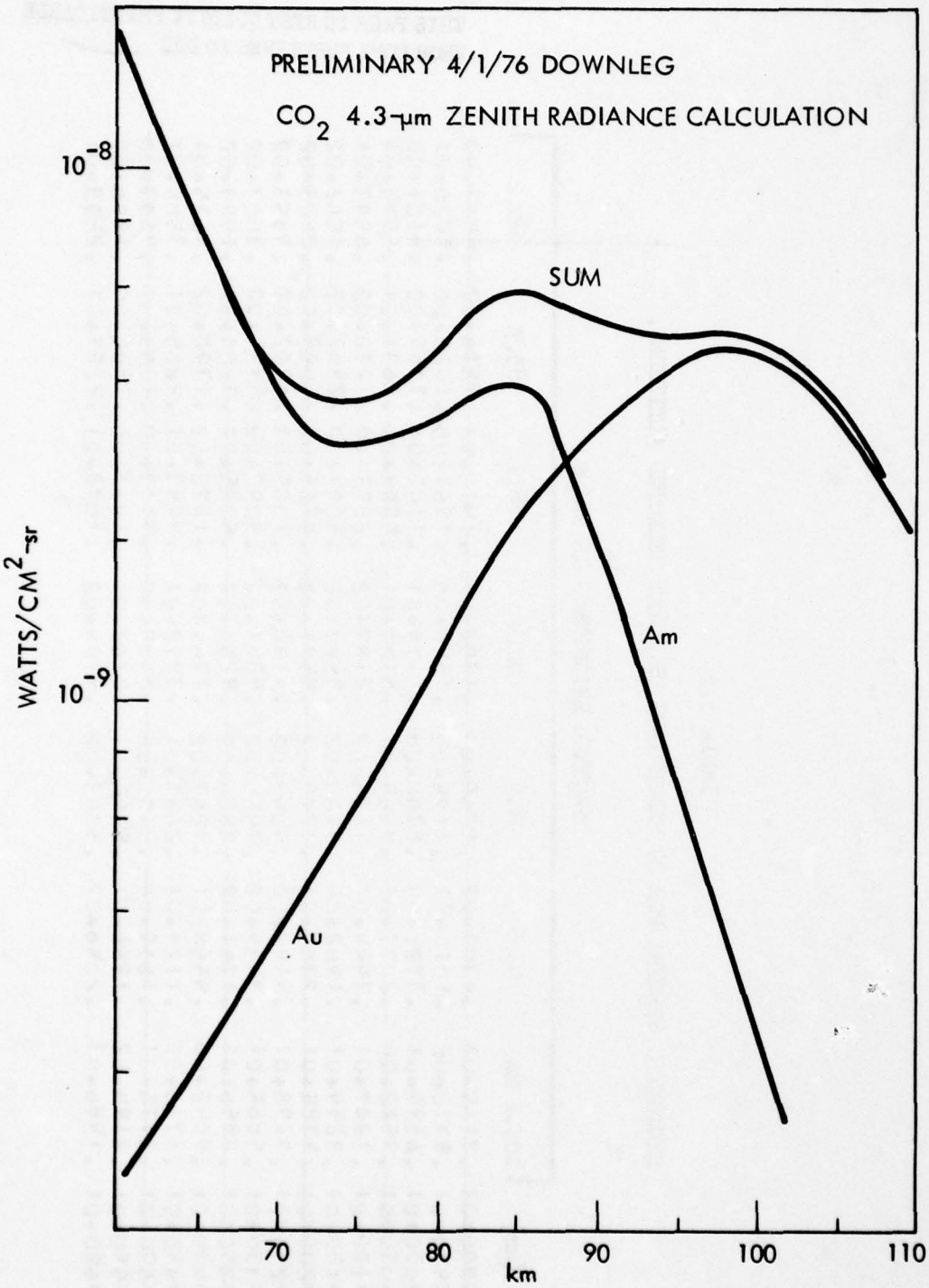

Figure 3-7. A preliminary version of the predicted auroral component A_u and the predicted ambient component A_m of downleg CO_2 4.3 μm zenith radiance on 1 April 1976 are shown here, the sum of the two is also shown.

and also includes the effect of $OH^{\ddagger}$ vv $N_2^{\ddagger}$. The downleg auroral component is calculated on the basis of a preliminary energy input model that we derived from the ground based blue and green scanning photometer data that are shown in reference 3-13. A two parameter fit similar to the BRIM model described in reference 3-1 was used to model the total deposition $\int dz q(z)$ and the altitude dependence of $q(z)$ from the blue and green photometric data. Corrections of the ground based photometric data for atmospheric extinction were applied on the basis of extinction data listed in reference 3-14. Only 5 minutes of photometric data taken prior to downleg penetration were given in reference 3-14 so our downleg auroral energy input model, which is based on these sparse data, should be considered <u>preliminary</u>.

The slit function for the HIRIS is given by reference 3-15.

$$F(w,w') = \frac{a}{\pi} (\sin(x)/x)^2$$

where $a = .4783\ \pi$ and $x = a(w-w')$. The HIRIS interferogram data are converted to spectral radiance at points w_n defined by $w_n = 626.51 + .96386\ n$. We performed our spectral radiance calculation for 3 sets of points w_n at four selected altitudes (66.6, 80.2, 94.9 and 107.1 km). The 3 sets of points w_n were selected to include the blue spike region, the transition region from strong to weak auroral emission lines in the r branch, and the red spike region. Synthetic spectra of the auroral component at altitudes z = 80.2, 94.9 and 107.1 km are shown on Figures 3-8. The dashed curves on Figure 3-8 are the weak band contribution ($2 \leq j \leq 11$) and the dotted curves the strong band contribution, the solid curve is the sum of the two, i.e. the total auroral spectral radiance. It is noteworthy that the weak bands dominate auroral emission in the red spike region.

By comparison of the prediction for the auroral spectral radiance near $w \leq 2278$ cm^{-1} (red spike region, $\lambda \geq 4.39$ μm) and $w \geq 2385$ cm^{-1} (blue spike, $\lambda \leq 4.19$ μm) with the strong R branch auroral spectral radiance near 2347 to 2376 cm^{-1} (4.26 to 4.21 μm) we see that a negligible fraction of CO_2 4.3 μm auroral emission from above 80 km may be expected to occur in the red and blue

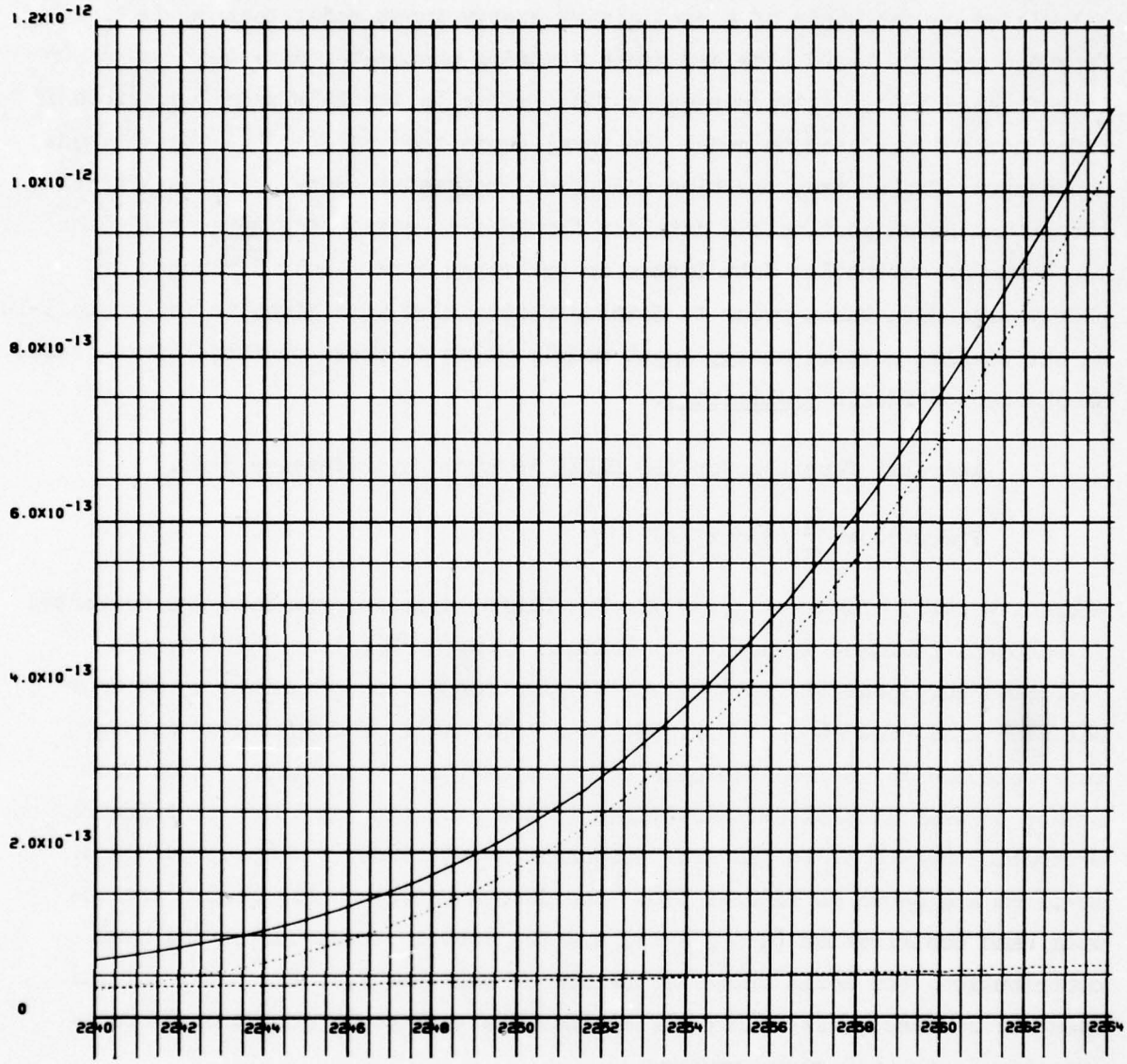

Figure 3-8a. The predicted downleg auroral contribution at altitude $z \simeq 107.1$ km to the zenith spectral radiance in the red band wing region obtained by HIRIS on 1 April 1976. The horizontal scale is in units cm^{-1}, the vertical scale in units w/cm^2 sr cm^{-1}. The dotted line is the contribution from the weak bands ($2 \leq j \leq 11$), the dashed line is the contribution from the strong band ($j = 1$). The solid line is the contribution from the sum of all the bands ($1 \leq j \leq 11$).

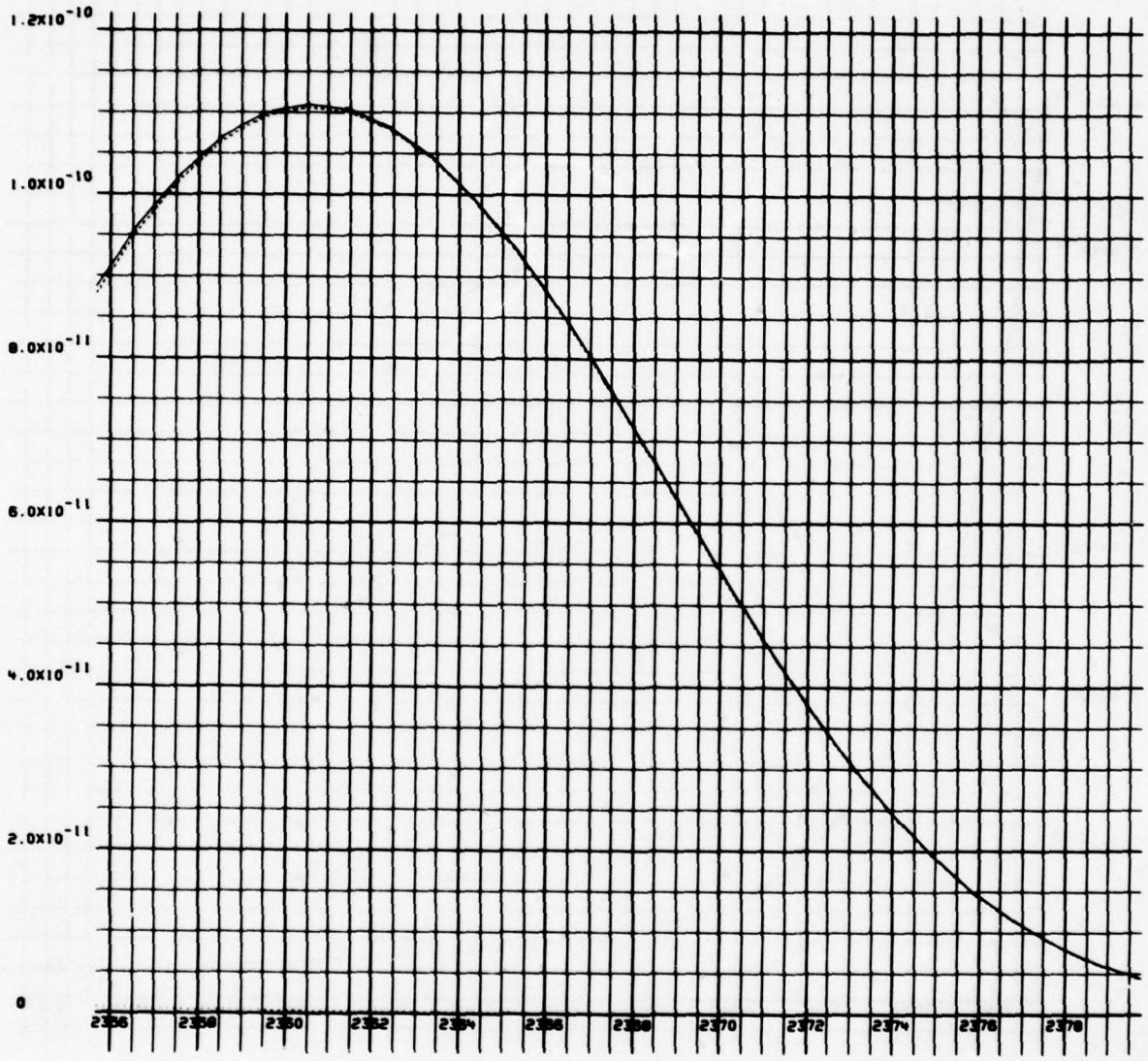

Figure 3-8b. Same as Figure 3-8a except for spectral region.

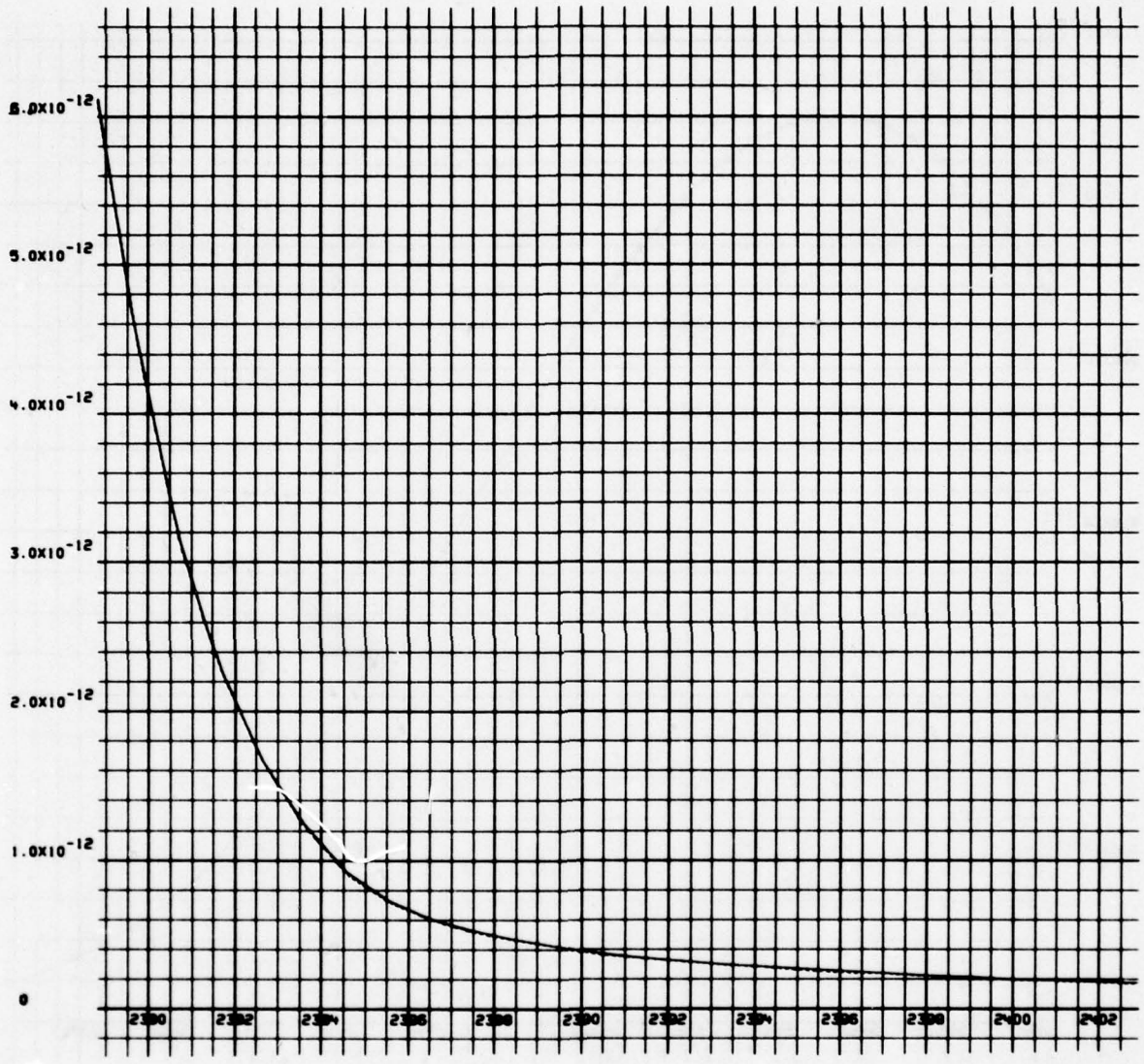

Figure 3-8c. Same as Figure 3-8a except for spectral region.

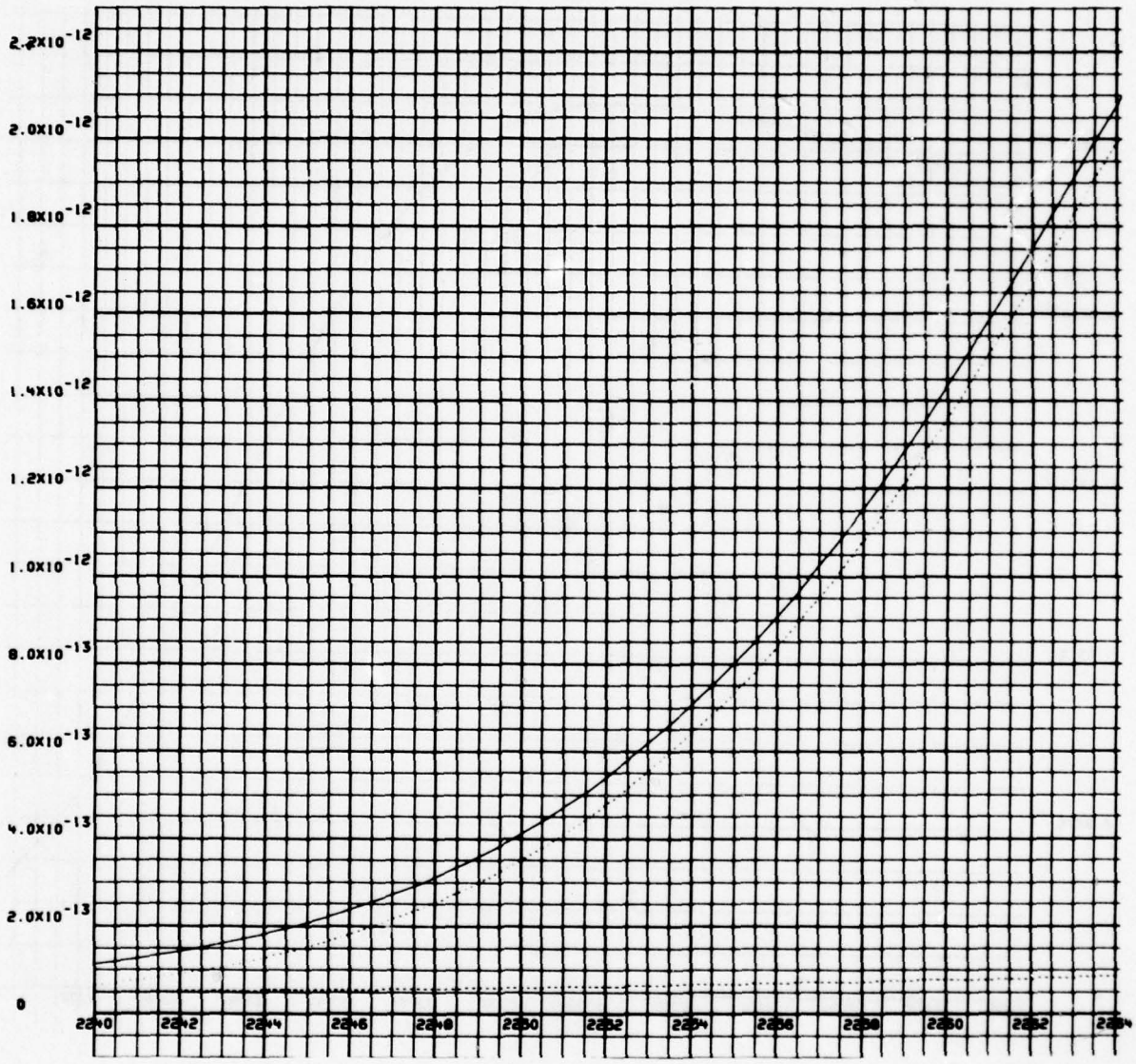

Figure 3-8d. Same as Figure 3-8a except the altitude is now 94.9 km.

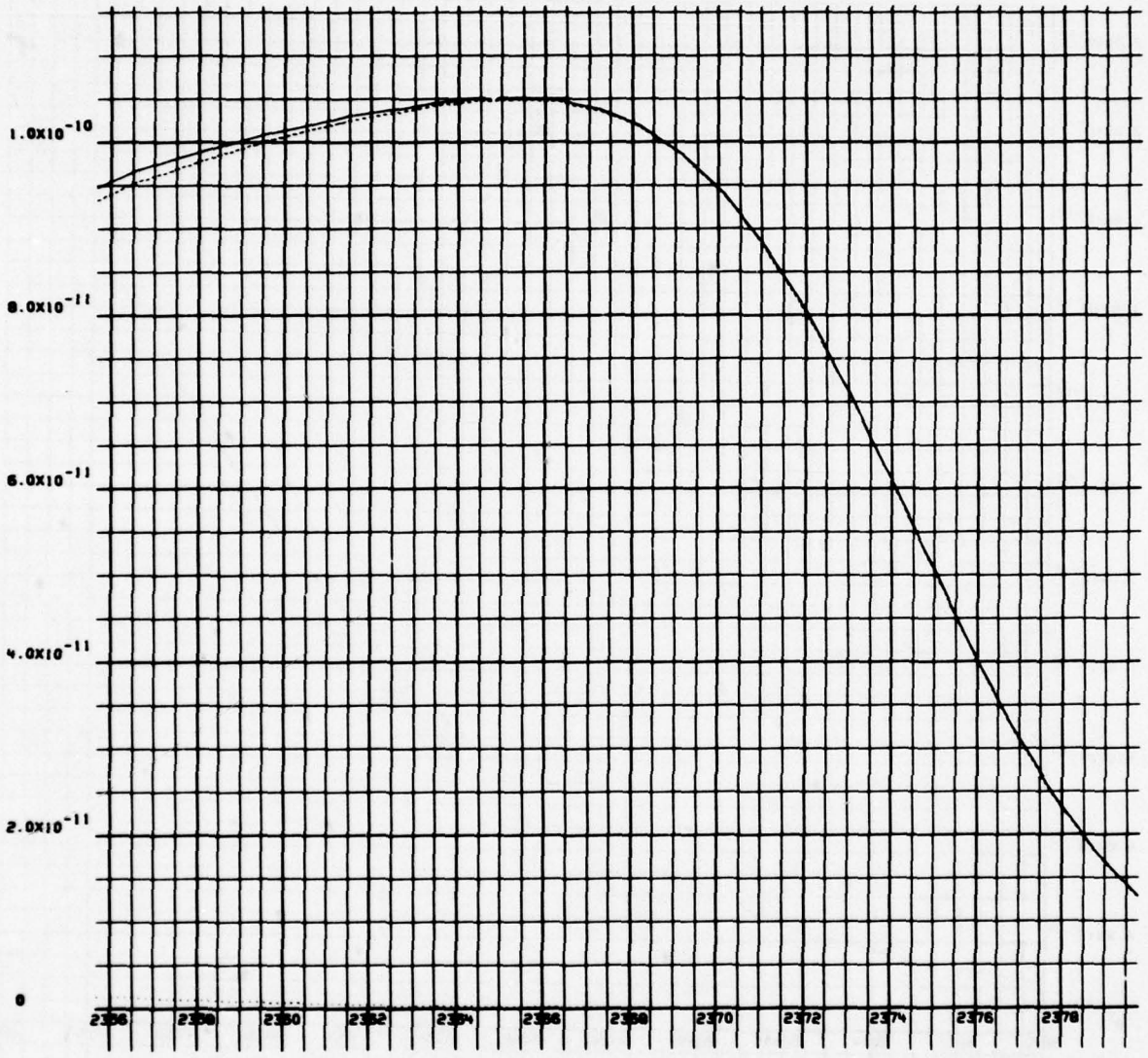

Figure 3-8e. Same as Figure 3-8d except for spectral region.

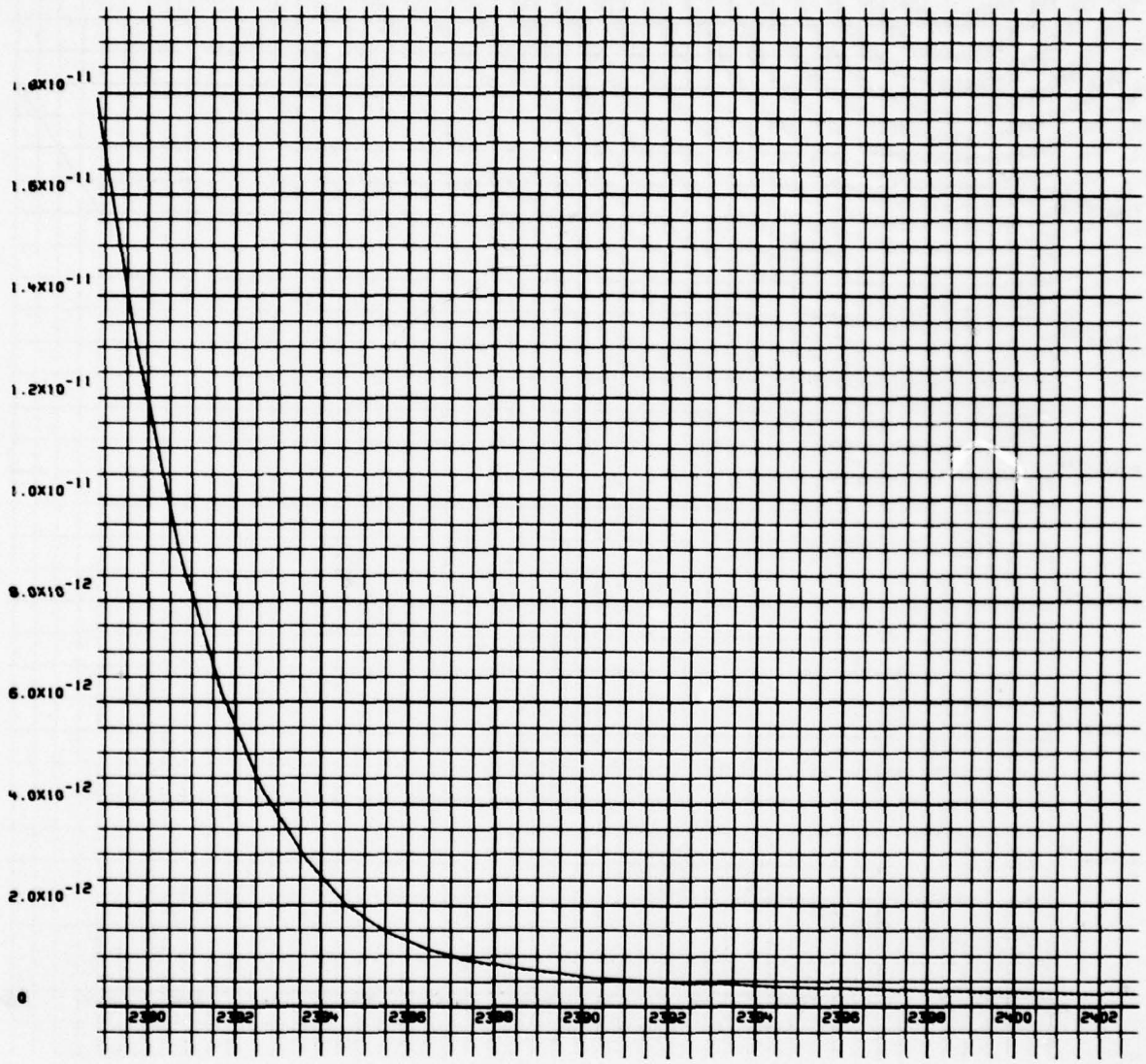

Figure 3-8f. Same as Figure 3-8d except for spectral region.

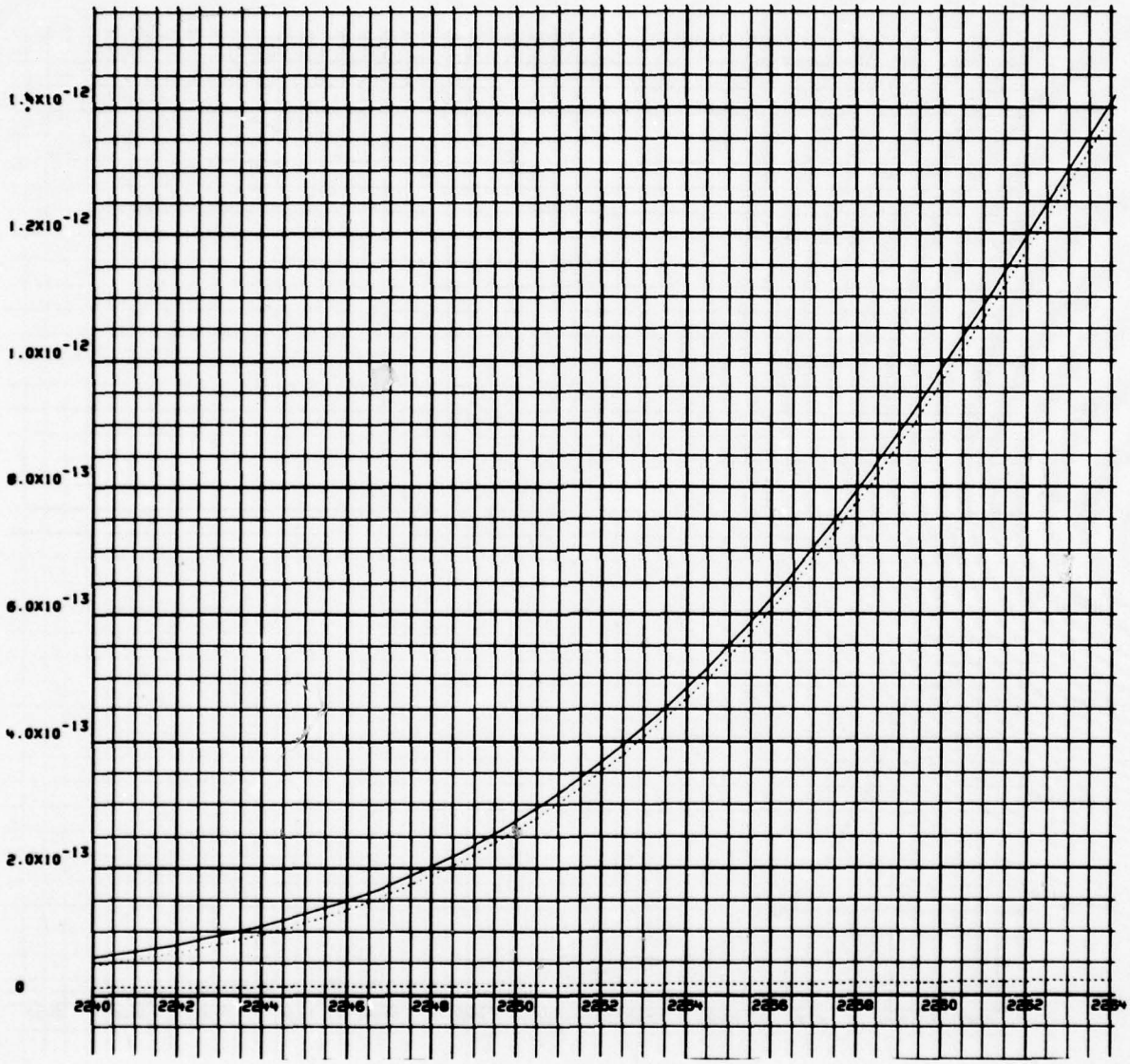

Figure 3-8g. Same as Figure 3-8a except the altitude is now 80.2 km.

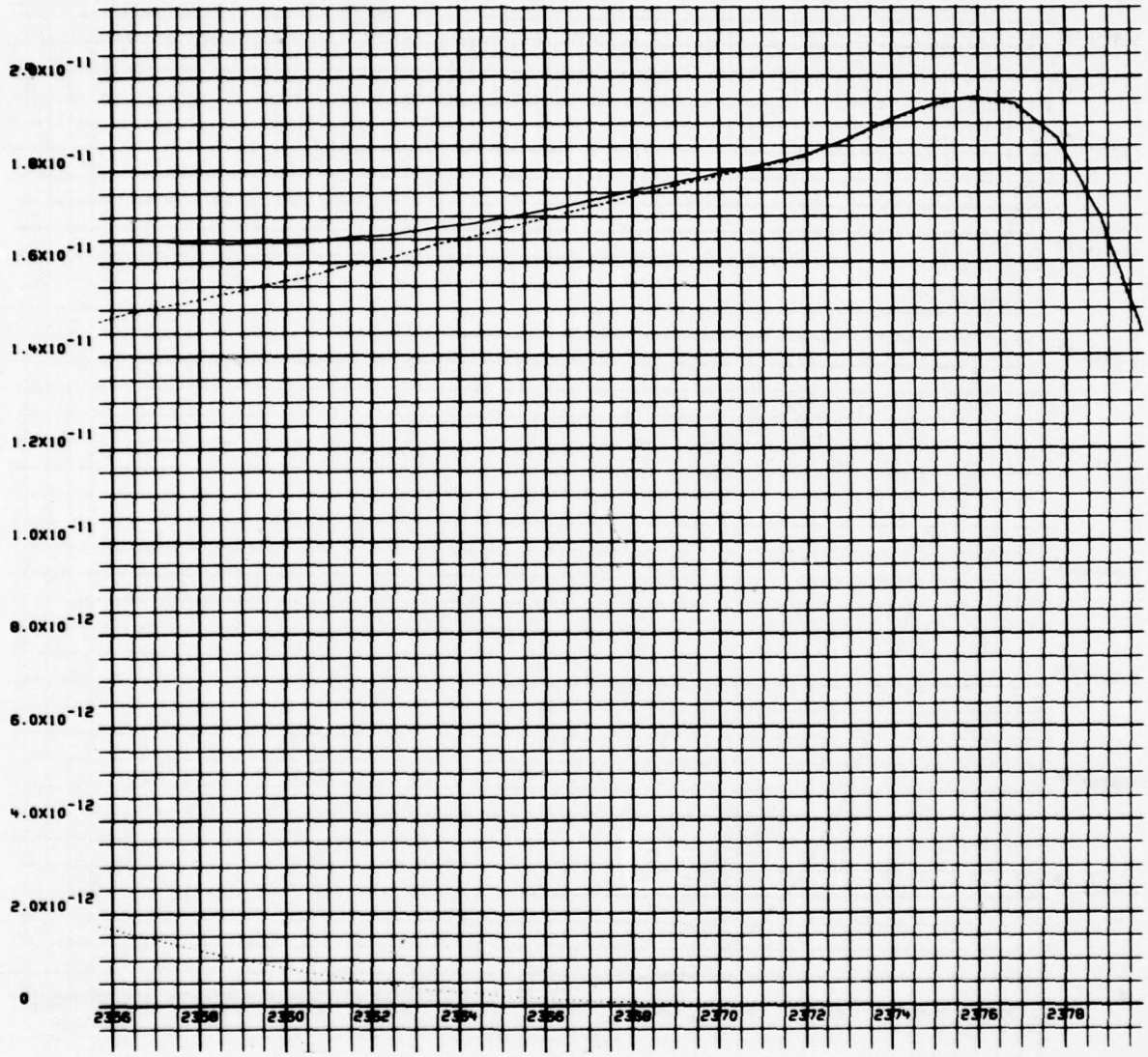

Figure 3-8h. Same as Figure 3-8g except for spectral region.

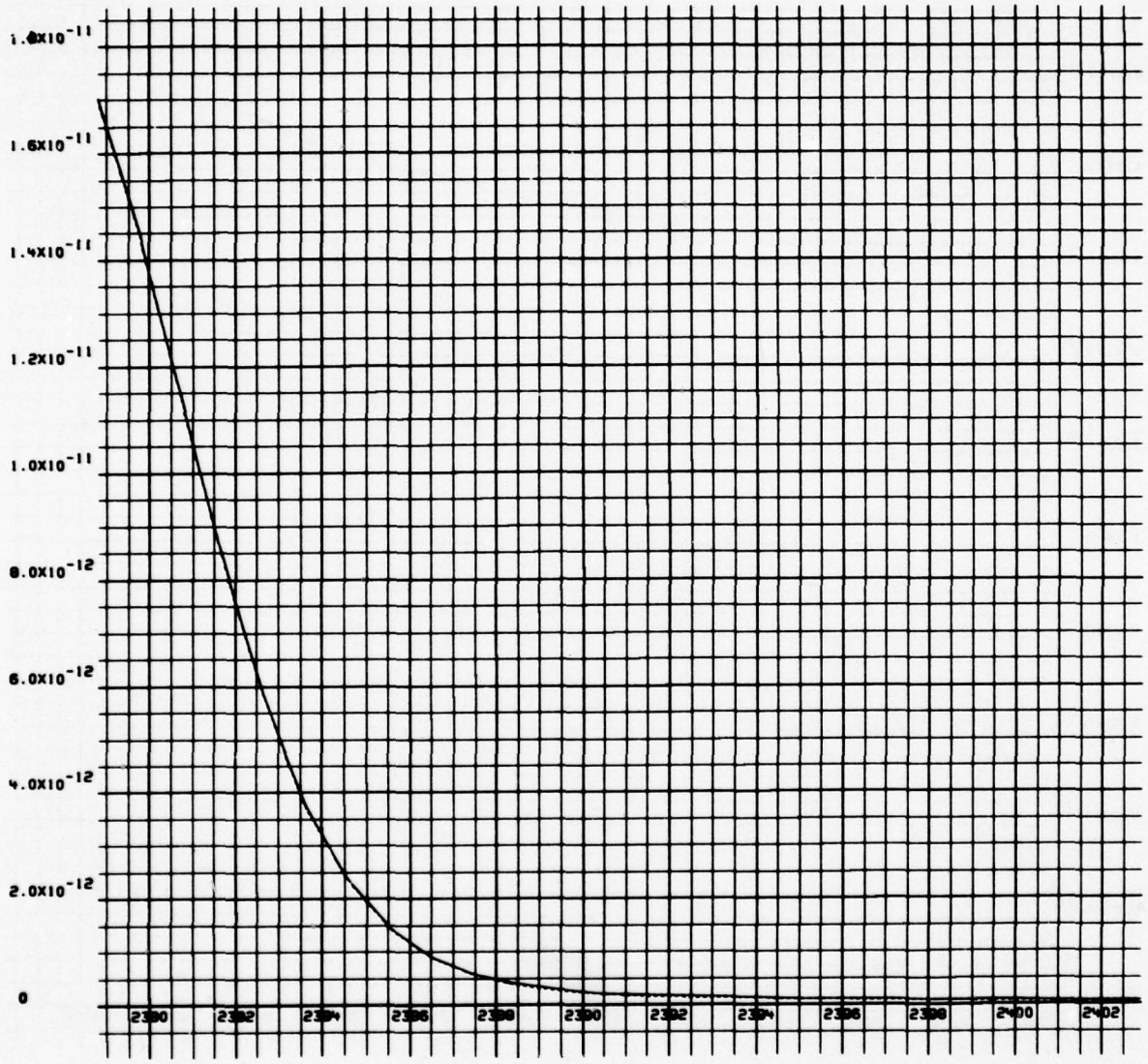

Figure 3-8i. Same as Figure 3-8g except for spectral region.

spike regions. The spectral characteristics of CO_2 4.3 μm emission above 80 km which would result from nuclear deposition may be expected to be similar.

The synthetic spectra for the ambient and auroral components of spectral zenith radiance near 66.6 km are shown on Figure 3-9. The weak band contribution to the red spike spectral radiance is noteworthy, as is the contribution to blue spike spectral radiance due to optical thickness broadening of the strong band. Thus for the case of nuclear deposition in the 60 to 70 km region we could expect a contribution to nadir spectral radiance near 4.198 μm that is qualitatively similar to the auroral blue spike which appears near $w = 2392\ cm^{-1}$ on Figure 3-9f. There would also be a comparatively strong weak band contribution to red spike nadir spectral radiance.

On Figure 3-10 we show a synthetic spectrum of the ambient zenith spectral radiance, calculated for z = 66.6 km, in the band origin spectral region. Figure 3-10 demonstrates that HIRIS-like resolution is sufficient to provide identification of the 626 001→000 band origin which occurs near 50 $2348.9\ cm^{-1}$ and of the 626 011→010 band origin and Q branch which occur near to $2336.4\ cm^{-1}$.

3.4 Implications

Our CO_2 4.3 μm spectral zenith radiance modeling effort in application to quiet night time SWIR CVF data obtained 11 April 1974 and to SWIR CVF data obtained in auroral breakup on 24 March 1973 has established two important points. First, excellent agreement is achieved with the data. This confirms that CO_2 is the principal emitter responsible for the 4.3 μm data feature. It confirms that we understand the quiet night time and auroral mechanisms that are responsible for the CO_2 emission well enough so that we can successfully model the data. Finally, it confirms that the spectral characteristics of the SWIR CVFs were accurately calibrated. Secondly, we have demonstrated that any feature which might appear in the region $\lambda \geq 4.5$ μm in data obtained with a SWIR CVF with resolution element width comparable to or less than that of the 11 April 1974 or 24 March 1973 CVF, will not be due to "cold" CO_2 emission.

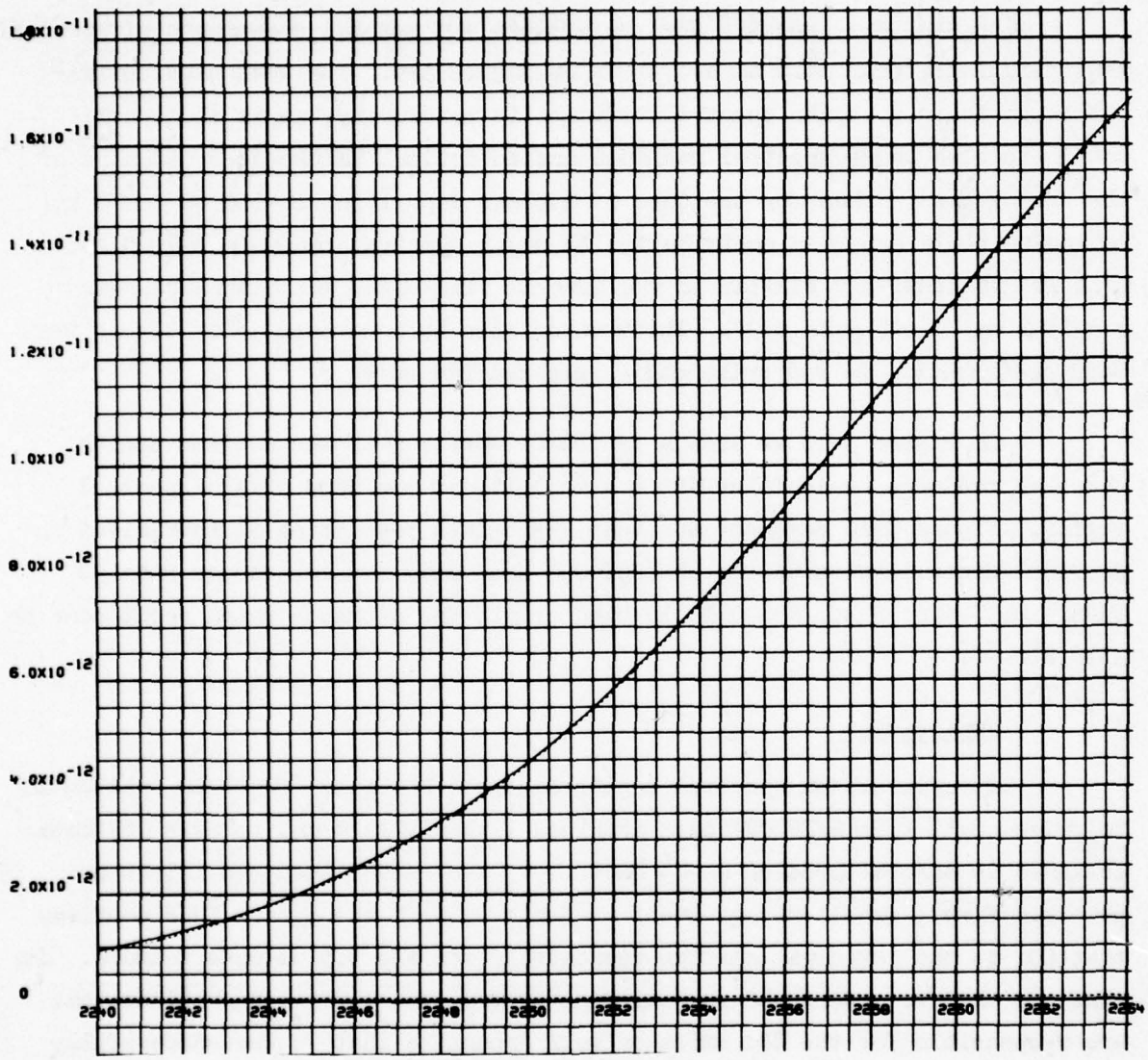

Figure 3-9a. Predicted ambient contribution to zenith spectral radiance at z = 66.6 km as measured by HIRIS on the downleg on 1 April 1976.

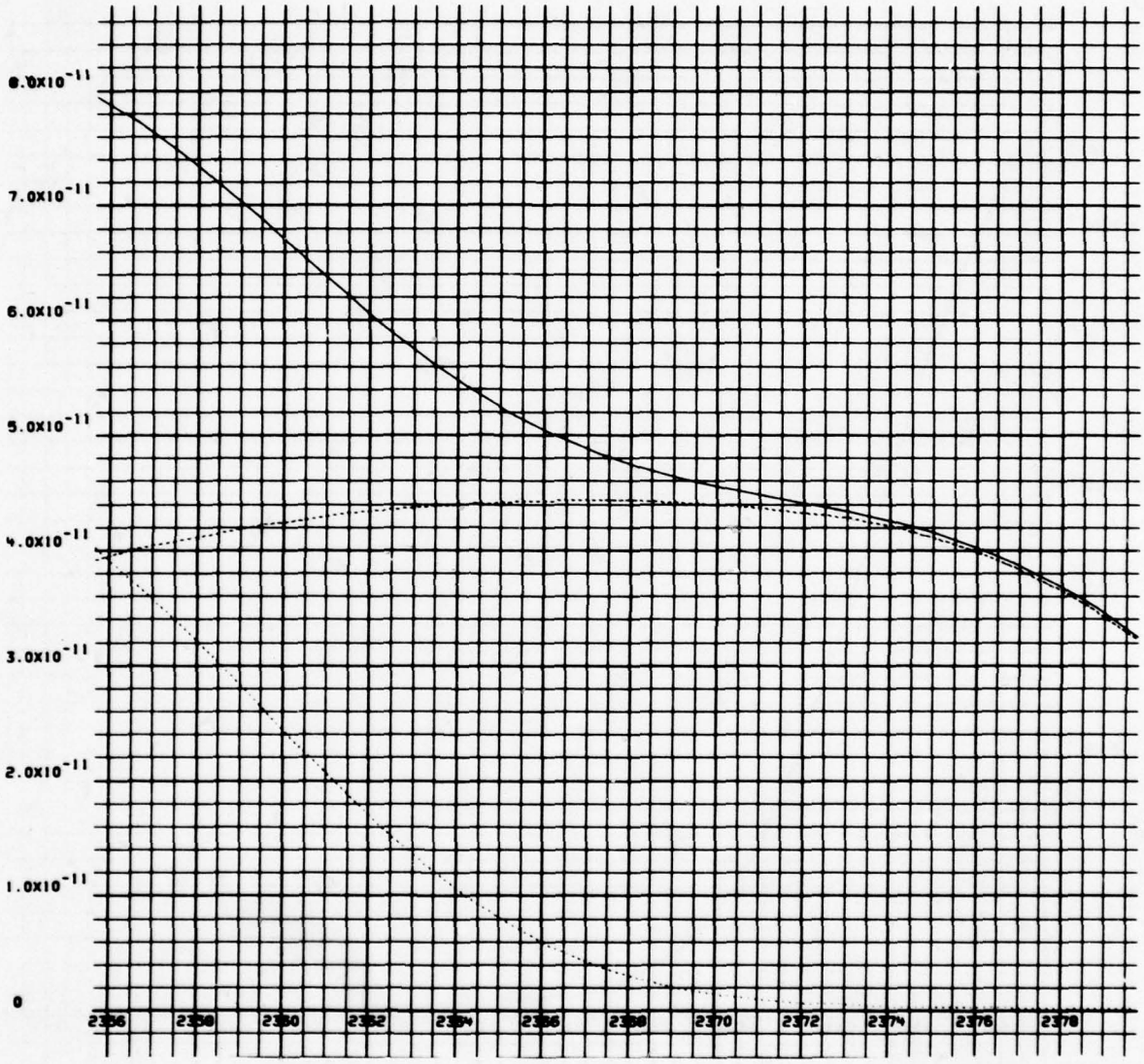

Figure 3-9b. Same as Figure 3-9a except for spectral region.

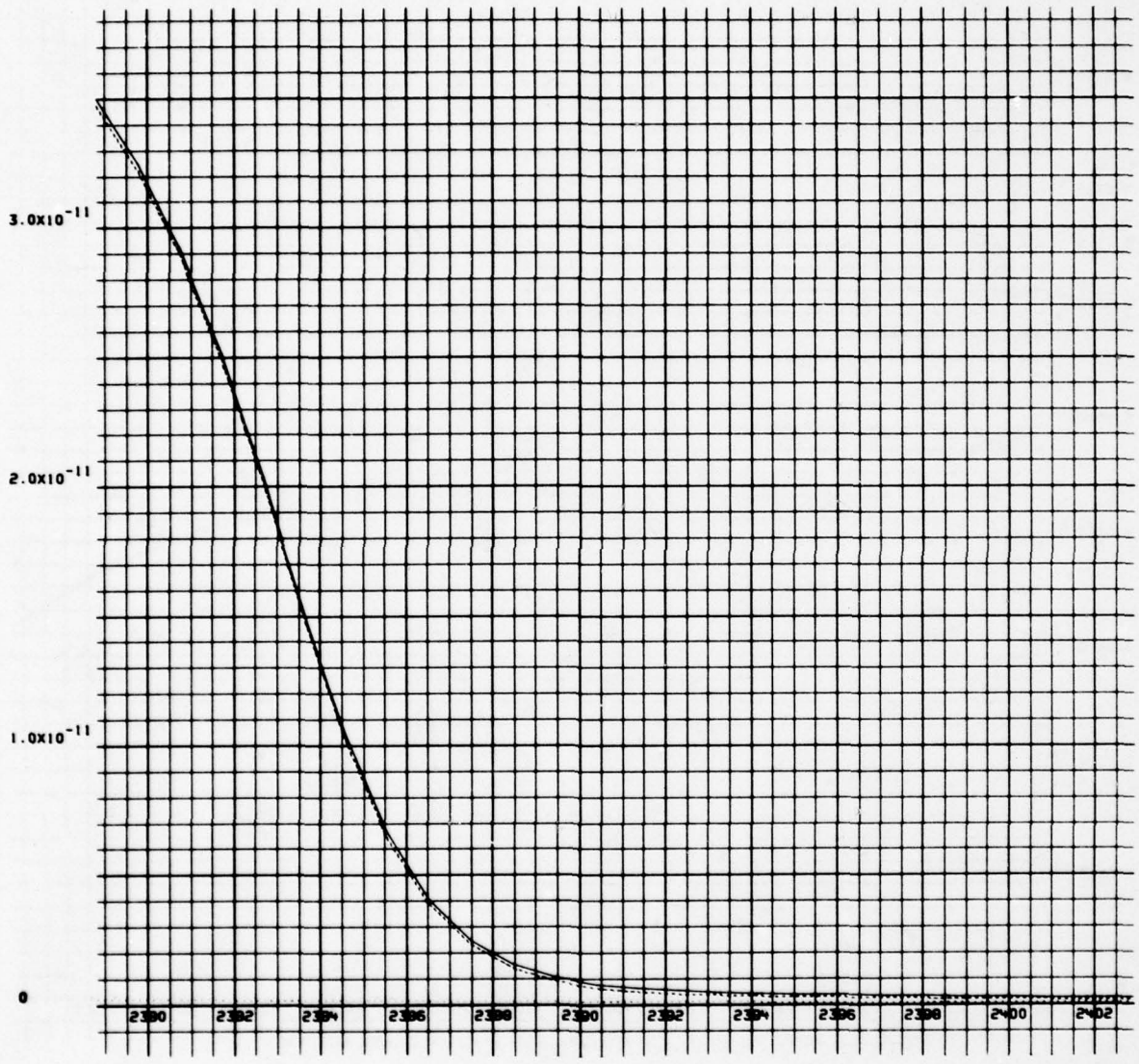

Figure 3-9c. Same as Figure 3-9a except for spectral region.

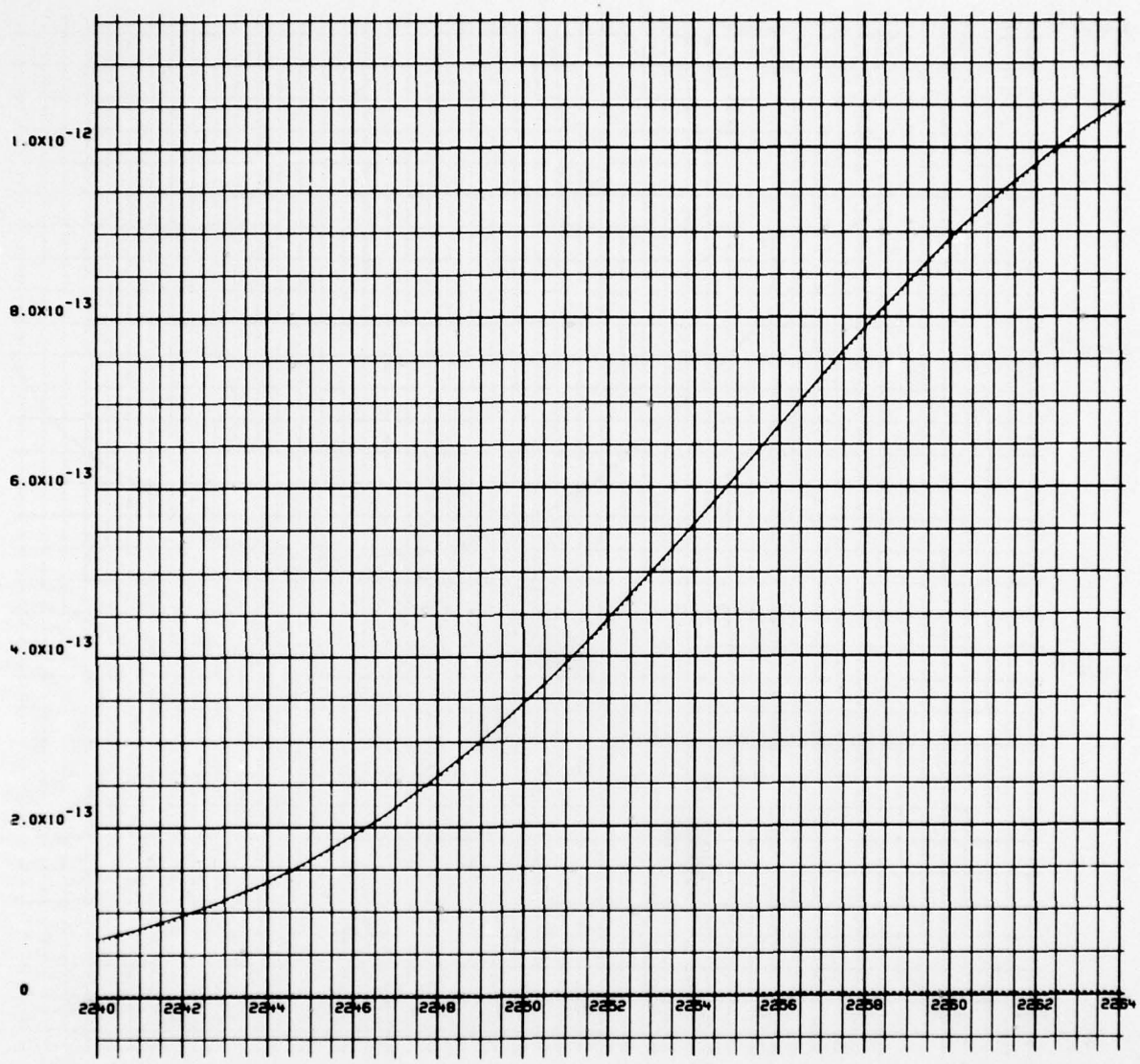

Figure 3-9d. Predicted auroral contribution to zenith spectral radiance measured at the downleg altitude z = 66.6 km by HIRIS on 1 April 1976.

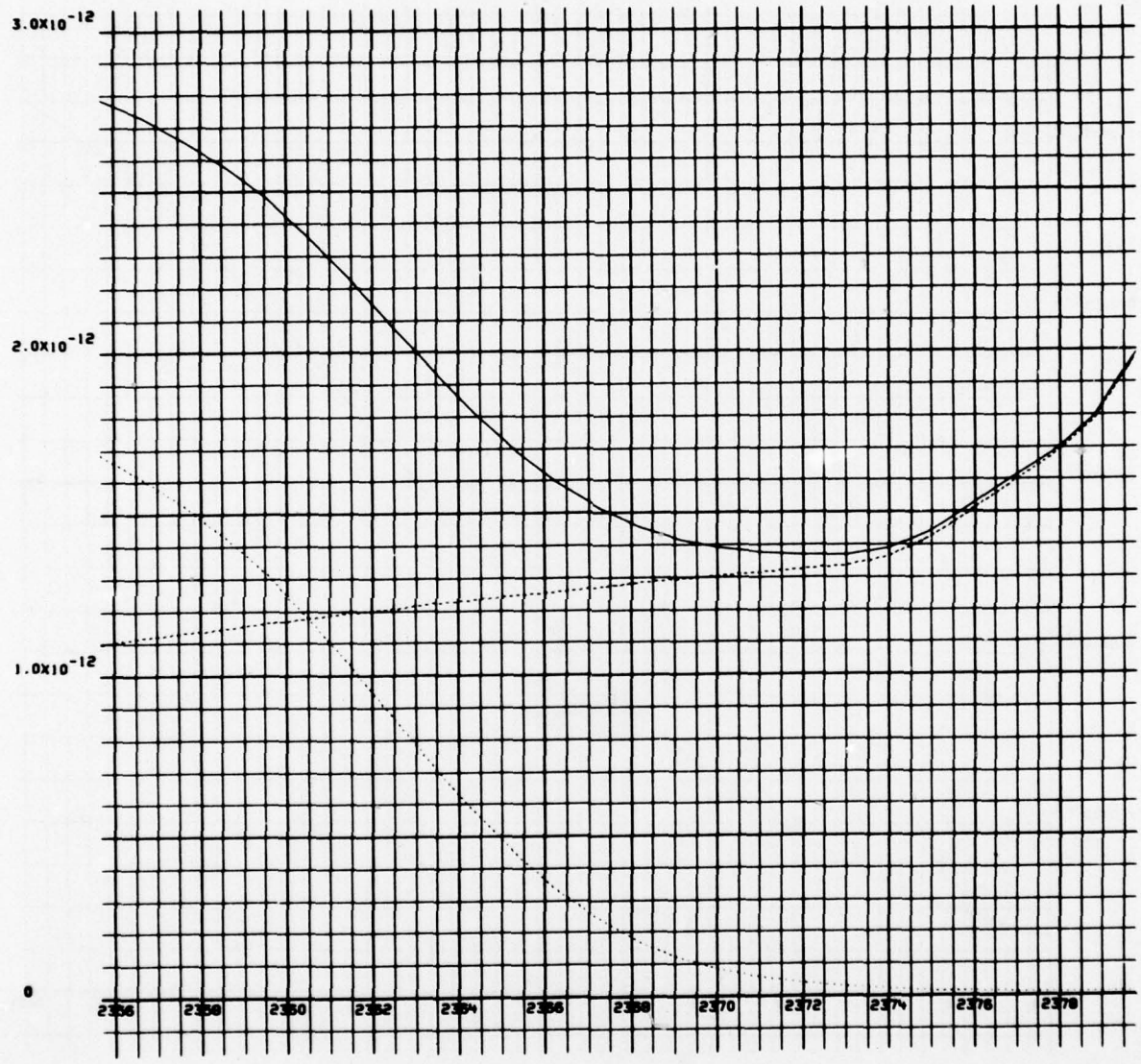

Figure 3-9e. Same as Figure 3-9d except for spectral region.

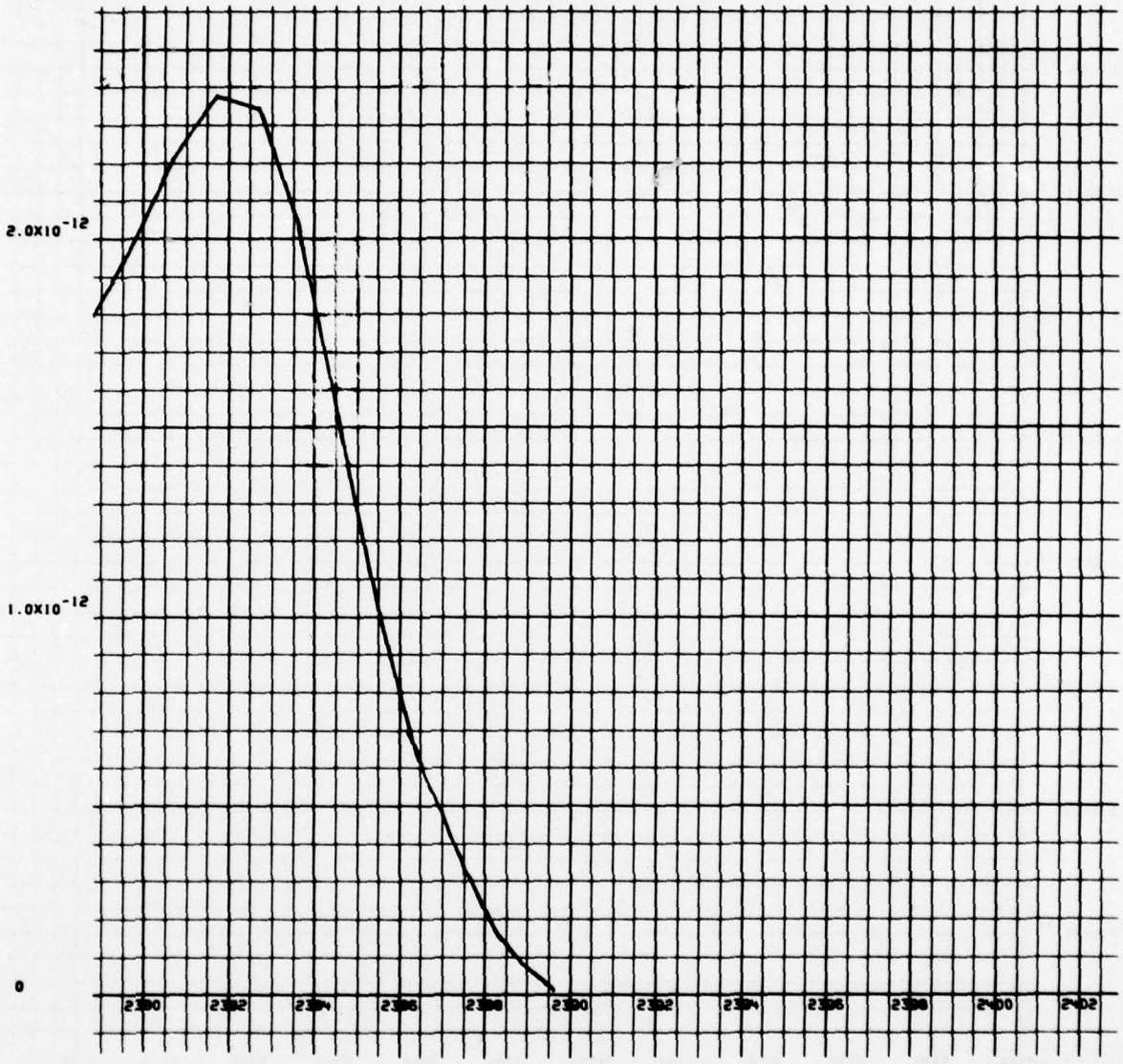

Figure 3-9f. Same as Figure 3-9d except for spectral region.

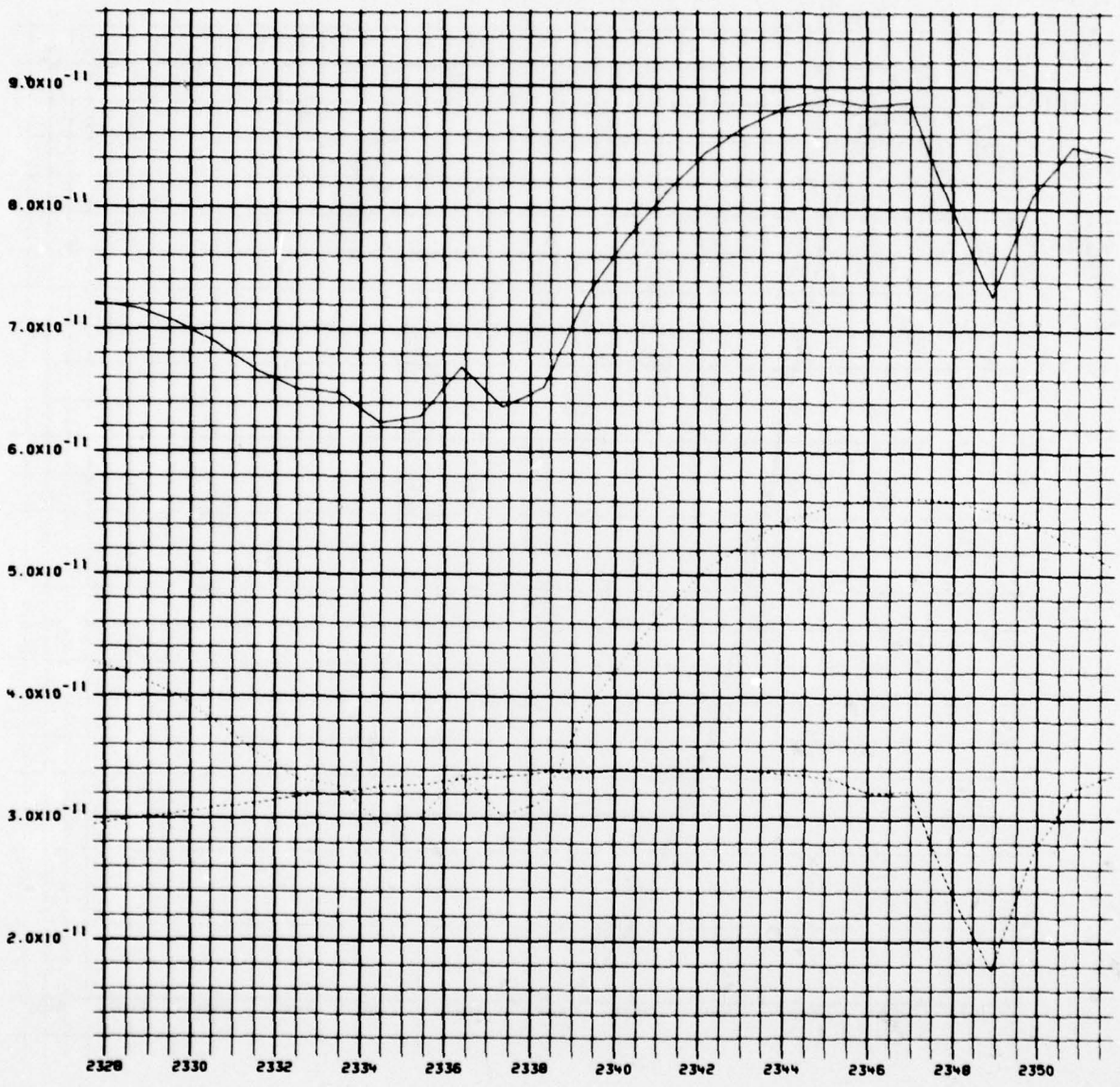

Figure 3-10. HIRIS synthetic spectrum of ambient spectral radiance in the band origin spectral region for altitude 66.6 km.

This second point is important since it may be used as another argument that CO_2 is not the emitter which is responsible for a possible auroral feature in the 4.5 to 4.6 μm region that was noted by Stair (reference 3-9) in SWIR CVF data obtained in a moderate aurora on 12 March 1975.

Our CO_2 4.3 μm spectral zenith radiance modeling effort in preliminary application to HIRIS data obtained 1 April 1976 has established the following points. First, HIRIS-like resolution is sufficient to observe the optical thickness induced change in the spectral shape of the CO_2 4.3 μm auroral spectral radiance as the rocket penetrates through the 80 to 110 km altitude region. Secondly, just a very small fraction of CO_2 emission above 80 km, be it auroral or nuclear induced, will occur in the red and blue spike regions. Thirdly, nuclear deposition in the 60 to 70 km regions should be expected to contribute to nadir radiance in both the red and blue spike regions. In the former due to weak band emission, in the latter due to the optical thickness band broadening effect. Finally, we have shown that HIRIS-like resolution should be sufficient to identify the 626 001→000 band origin, and the 626 011→010 band origin and Q branch in zenith spectral radiance data obtained at altitudes $z \leq 70$ km in ambient conditions.

3.5 References

3-1 Kumer, J. B., "Further Evaluation of ICECAP Auroral 4.3 μm Zenith Radiance," DNA 4260F, HAES Report No. 57, 1976

3-2 Kumer, J. B., "Theory of the CO_2 4.3 μm Aurora and Related Phenomena," J. Geophys. Res. 82, 2203, 1977

3-3 Kumer, J. B., "Analysis of 4.3 μm ICECAP Data," AFCRL-TR-74-0334, HAES Report No. 19, 1974

3-4 Kumer, J. B. and T. C. James, "CO_2 and N_2 Vibrational Temperatures in the $50 \leq z \leq 130$ km Altitude Region," J. Geophys. Res. 79, 638, 1974

3-5 Herzberg, G., Molecular Spectra and Molecular Structure I. Spectra of Diatomic Molecules, published by D. Van Nostrand Co., Inc., 1950

3-6 McClatchey, R. A., W. S. Benedict, S. A. Clough, D. E. Burch, R. F. Calfee, K. Fox, L. S. Rothman and J. S. Garing, "AFCRL Atmospheric Absorption Line Parameters Compilation," AFCRL-TR-73-0096, 1973

3-7 Wheeler, N. B., A. T. Stair, Jr., G. Frodsham and D. J. Baker, "Rocket Borne Spectral Measurement of Atmospheric Infrared Emission During A Quiet Condition in the Auroral Zone," AFGL-TR-76-0252, HAES Report No. 32, 1976

3-8 Kumer, J. B., A. T. Stair, Jr., N. B. Wheeler, K. D. Baker and D. J. Baker, "Evidence for an $OH^{\ddagger} \overset{VV}{\rightarrow} N_2^{\ddagger} \overset{VV}{\rightarrow} CO_2(\nu_3) \rightarrow CO_2 + h\nu(4.3\ \mu m)$ Mechanism for 4.3 μm Airglow," submitted for publication November 1977 to J. Geophys. Res.

3-9 Stair, A. T. Jr., "HAES Overview and Review of the IR Spectral Measurements," Presentation given at the HAES Infrared Data Review Meeting 13-15 June 1977 at Falmouth, Mass. and documented in AFGL-OP-TM-05, 1977

3-10 Baker, K. D., D. J. Baker, J. C. Ulwick and A. T. Stair, Jr., "Measurements of 1.5 to 5.3 μm Infrared Enhancements Associated with a Bright Auroral Breakup," J. Geophys. Res. 82, 3518, 1977

3-11 Kemp, John, Private Communication, Nov. 1977

3-12 Stair, A. T., Jr., J. C. Ulwick, K. D. Baker and D. J. Baker, "Rocket Borne Observations of Atmospheric Infrared Emissions in the Auroral Zone," Atmospheres of the Earth and Planets, Edited by Billy M. McCormac, published by D. Reidel Publishing Co., Dordrecht-Holland, p 335, 1975

3-13 Stair, A. T., Jr., J. W. Rogers and W. R. Williamson, "HIRIS Experiment," Quick Look Data Report AFGL-OP-TM-02, 15 April 1976

3-14 Elterman, L., "UV, Visible and IR Attenuation for Altitudes to 50 km, 1968," AFCRL-68-0153, 1968

3-15 Private Communication, AFGL personnel

4.0 CONCLUSIONS AND RECOMMENDATIONS

4.1 CO_2 Fluorescence

The measurements which have been described in Section 2 of this report indicate the importance of accounting for the frequency response of the 4.3 μm emission when CO_2 is irradiated with a sinusoidal radiation source at 2.7 μm. The results of our analysis yield quenching rate constants and energy transfer rate constants which are consistent with existing literature. Further refinement of the techniques used in our experiments should lead to a simple and accurate method of obtaining these rate constants.

From the observed frequency response of the CO_2 plus rare gas mixtures studied, there does not appear to be a significant contribution to the 4.3 μm emission from the fluorescence bands 021-020 and 101-100. On the other hand, our transmission measurements yield results which could be interpreted to indicate some contribution from the fluorescence bands. Until such time as detailed calculations are made which include multiple scattering and internal reflections in the fluorescence and absorption cells, the interpretation of the transmission measurements is uncertain.

The results of our experiments lead to the conclusion that because of the very rapid transfer of ν_3 excitation from the levels 021 and 101 to ground state CO_2 to form the level 001, that a laser excitation source at 2.7 μm is a better technique for observing the direct fluorescence.

Based on the results of the present study, we can make a number of recommendations for further work. These are listed below:

1) Utilize a Pulsed Tunable laser at 2.7 μm to produce the 4.3 μm fluorescence bands 021-020 and 101-100 and observe the decay at very short time intervals following excitation.

2) Obtain additional measurements of the Intensity of Fluorescence as a function of chopping frequency for various CO_2, N_2 and rare gas mixtures.

3) Improve the data evaluation techniques, particularly for situations involving N_2 where there are several rate constants to be extracted from a limited number of data points.

4) Based on the results of (2) and (3), develop a detailed treatment of the accuracy of this technique for obtaining rate constants.

5) Extend the measurements (2) to include the out-of-phase component to the fluorescence and verify the consistency of the rate constants obtained by the ratio of the in-phase to out-of-phase intensities.

6) Study the variation of transmission measurements with chopping frequency and measure the frequency response of the intensity after an absorption cell is placed between the fluorescence cell and the detector which may provide some indication of differences in decay rates for different 4.3 μm bands.

4.2 Modelling of CO_2 4.3 μm Spectral Structure

Our CO_2 4.3 μm spectral zenith radiance modeling effort in application to quiet night time SWIR CVF data obtained 11 April 1974 and to SWIR CVF data obtained in auroral breakup on 24 March 1973 has established two important points. First, a good enough agreement is achieved with the data to confirm that CO_2 is the principal emitter responsible for the 4.3 μm data feature, and to confirm that we understand the quiet night time and auroral mechanisms that are responsible for the CO_2 emission well enough so that we can model the data. It also confirms that the spectral characteristics of the SWIR CVFs were calibrated fairly accurately. Secondly, we have demonstrated that any feature which might appear in the region $\lambda \geq 4.5$ μm in data obtained with a SWIR CVF with resolution element width comparable to or less than that of the 11 April 1974 or 24 March 1973 CVF, will not be due to 'cold' CO_2 emission. This second point is important since it may be used as another

argument that CO_2 is not the emitter which is responsible for a possible auroral feature in the 4.5 to 4.6 μm region that was noted by Stair in SWIR CVF data obtained in a moderate aurora on 12 March 1975.

Our CO_2 4.3 μm spectral zenith radiance modeling effort in preliminary application to HIRIS data obtained 1 April 1976 has established the following points. First, HIRIS-like rsolution is sufficient to observe the optical thickness induced change in the spectral shape of the CO_2 4.3 μm auroral spectral radiance as the rocket penetrates through the 80 to 110 km altitude region. Secondly, just a very small fraction of CO_2 emission above 80 km, be it auroral or nuclear induced, will occur in the red and blue spike regions. Thirdly, nuclear deposition in the altitude region below 30 km should also be expected to contribute to nadir radiance in both the red and blue spike regions. In the former, due to weak band emission; in the latter, due to the optical thickness band broadening effect. Finally, we have shown that HIRIS-like resolution should be sufficient to identify the 626 001-000 band origin and Q branch in zenith spectral radiance data obtained at altitudes $z \lesssim 70$ km.

Our recommendation for improved modelling of the spectral structure in the quiescent, auroral and nuclear disturbed infrared background would include:

- Upgraded modelling in the 4.3 μm region by including the emitters NO^+, N_2O, CO and $^{14}N^{15}N$ in the model.

- Extend the modelling capability to other spectral regions by incorporating emitters and emission mechanisms roughly as are listed below:

Spectral Region	Emitter	Mechanism
2.7 μm	NO	$N(^2D) + O_2 \longrightarrow NO(v)$
	OH	Nightglow Mechanism
	OH	Dayglow Mechanism
	CO_2, H_2O	Solar Scattering
	CO_2	Auroral 2.7 μm Mechansim?
5.3 μm	NO	$N(^2D) + O_2$
6.3 μm	H_2O	Non-LTE Thermal Solar Scattering

Spectral Region	Emitter	Mechanism
9-11 μm	O_3	Non-LTE Thermal and $O + O_2 + M \longrightarrow O_3^{\ddagger}$
$\lambda \gtrsim 12.5$ μm	CO_2	Non-LTE Thermal
$\lambda \gtrsim 16$ μm	N_2O	Non-LTE Thermal and $N_2(A) + O_2 \longrightarrow N_2O^{\ddagger}$

- Validate the improved spectral models by comparison with rocket-borne CVF and interferometer (HIRIS, FWI) measurements of zenith and limb (SPIRE) spectral radiance, by comparison with laboratory measured (LABCEDE, COCHISE and our own facility, for example) spectral radiances, and also by comparison with EXCEDE spectral radiance measurements.

DISTRIBUTION LIST

DEPARTMENT OF DEFENSE

Director
Defense Advanced Rsch. Proj. Agency
ATTN: LTC W. A. Whitaker
ATTN: Strategic Technology Office
ATTN: Nuclear Monitoring Research

Defense Documentation Center
Cameron Station
12 cy ATTN: TC

Director Defense Nuclear Agency
ATTN: TISI Archives
ATTN: RAAE, MAJ John Clark
ATTN: RAEV, Harold C. Fitz, Jr.
ATTN: DDST
ATTN: RAAE, MAJ James W. Mayo
3 cy ATTN: TITL, Tech. Lib.
2 cy ATTN: RAAE, Charles A. Blank

Commander
Field Command
Defense Nuclear Agency
ATTN: FCPR

Chief
Livermore Divison, Fld. Command DNA
Lawrence Livermore Laboratory
ATTN: FCPRL

Under Secy. of Def. for Rsch. & Engrg.
ATTN: S&SS(OS)

DEPARTMENT OF THE ARMY

Commander/Director
Atmospheric Sciences Laboratory
U.S. Army Electronics Command
ATTN: DELAS-AE-M, F. E. Niles
ATTN: H. Ballard
ATTN: DRSEL-BL-SY-S, D. Snider
ATTN: R. Rosen

Commander
Harry Diamond Laboratories
2 cy ATTN: DELHD-NP, F. N. Wimenitz

Commander
U.S. Army Nuclear Agency
ATTN: MONA-WE, J. Berberet

Director
BMD Advanced Tech. Center
ATTN: ATC-O, W. Davies
ATTN: ATC-T, Melvin T. Capps

Dep. Chief of Staff for Rsch. Dev. & Acq.
ATTN: NCB Division
ATTN: DAMA-CSZ-C
ATTN: Dama-WSZ-C

Chief of Engineers
ATTN: Fernand DePersin

DEPARTMENT OF THE ARMY (Continued)

Dep. Chief of Staff for Ops. & Plans
ATTN: DAMO-DDL, COL D. W. Einsel
ATTN: Div. of Chem. & Nuc. Ops.

Director
U.S. Army Ballistic Research Labs.
ATTN: Tech. Lib., E. Baicy
ATTN: John Mester
ATTN: J. Heimerl
ATTN: M. Kregl

Commander
U.S. Army Electronics Command
ATTN: DRSEL-PL-ENV, Hans A. Bomke
ATTN: DRSEL
ATTN: Stanley Kronenberg
ATTN: DRSEL-RD-P
ATTN: DRSEL-TL-IR, E. T. Hunter
ATTN: Inst. for Exploratory Rsch.
ATTN: Weapons Effects Section

Commander
U.S. Army Foreign Science & Tech. Ctr.
ATTN: Robert Jones

Commander
U.S. Army Material Dev. & Rdns. Cmd.
ATTN: DRXCD-TL
ATTN: DRCCDC, J. A. Bender

Commander
U.S. Army Missile Command
ATTN: DRSMI-ABL
ATTN: Chief, Doc. Section
ATTN: DRSMI-XS, Chief Scientist

Chief
U.S. Army Research Office
ATTN: CRDARD-CCS, Hermann Robl
ATTN: CRDARD-P, Robert Mace

DEPARTMENT OF THE NAVY

Chief of Naval Research
ATTN: Code 421, B. R. Junker
ATTN: Code 461, Jacob Warner
ATTN: Code 461, R. G. Joiner

Commander
Naval Ocean Systems Center
ATTN: Code 2200 1, Verne E. Hildebrand
ATTN: Code 2200, Ilan Rothmuller
ATTN: Code 2200, Jurgan Richter
ATTN: Code 2200, William F. Moler
ATTN: Code 2200, Richard Pappert
ATTN: Tech. Lib. for T. J. Keary
ATTN: Code 2200, Herbert Hughes

Superintendent (Code 1424)
Naval Postgraduate School
ATTN: Code 2124, Tech. Reports Librarian

DEPARTMENT OF THE NAVY (Continued)

Director
Naval Research Laboratory
ATTN: Douglas P. McNutt
ATTN: Code 7701, Jack D. Brown
ATTN: Code 7709, Wahab Ali
ATTN: Code 7750, Darrell F. Strobel
ATTN: Code 7700, Timothy P. Coffey
ATTN: Code 7750, Paul Juluenne
ATTN: Code 2600, Tech. Lib.
ATTN: Code 7127, Charles Y. Johnson
ATTN: Code 7120, W. Neil Johnson
ATTN: Code 7750, J. Davis
ATTN: Code 7750, Klaus Hein
ATTN: Code 7750, Joel Feddler
ATTN: Code 2027, Tech. Lib.
ATTN: Code 7750, S. L. Ossakow
ATTN: Code 7730, Edgar S. McClean

Officer-in-Charge
Naval Surface Weapons Center
ATTN: Code WA501, Navy Nuc. Prgms. Off.
ATTN: Code WX21, Tech. Lib.
ATTN: D. J. Sand
ATTN: L. Rudlin

Commanding Officer
Naval Intelligence Support Center
ATTN: Doc. Con.
ATTN: Code 40A, E. Blase

Commander
Naval Weather Service Command
ATTN: Mr. Martin

DEPARTMENT OF THE AIR FORCE

AF Geophysics Laboratory, AFSC
5 cy ATTN: OPR, Alva T. Stair
5 cy ATTN: LKB, Kenneth S. W. Champion
2 cy ATTN: OPR-1, R. Murphy
2 cy ATTN: OPR-1, J. Kennealy
5 cy ATTN: OPR, J. Ullwick

AF Weapons Laboratory, AFSC
ATTN: CA
ATTN: Col G. J. Freyer
2 cy ATTN: DYM
5 cy ATTN: DYC
5 cy ATTN: SUL
5 cy ATTN: DYT

Commander
ASD
ATTN: ASD-YH-EX, Lt Col Robert Leverette

SAMSO/SZ
ATTN: SZJ, Maj Lawrence Doan

AFTAC
5 cy ATTN: TD
2 cy ATTN: Tech. Lib.

Hq. USAF
ATTN: DLS
ATTN: DLCAW
ATTN: DTL
ATTN: DLXP
ATTN: SDR
ATTN: Tech. Lib.

DEPARTMENT OF THE AIR FORCE (Continued)

SAMSO/AW
ATTN: AW

DEPARTMENT OF ENERGY

Division of Military Application
ATTN: Doc. Con. for Major D. A. Haycock
ATTN: Doc. Con. for Colonel T. Gross
ATTN: Doc. Con. for David Slade
ATTN: Doc. Con. for Donald I. Gale
ATTN: Doc. Con. for F. S. Ross

Los Alamos Scientific Laboratory
ATTN: Doc. Con. for R. A. Jeffries
ATTN: Doc. Con. for C. R. Mehl
ATTN: Doc. Con. for G. Rood
ATTN: Doc. Con. for H. V. Sego
ATTN: Doc. Con. for D. Steinhaus
ATTN: Doc. Con. for J. Judd
ATTN: Doc. Con. for T. Bieniewski
ATTN: Doc. Con. for D. M. Rohrer
ATTN: Doc. Con. for Martin Tierney
ATTN: Doc. Con. for Marge Johnson
ATTN: Doc. Con. for John S. Malik
ATTN: Doc. Con. for William Maier
ATTN: Doc. Con. for S. Rockwood
ATTN: Doc. Con. for Donald Kerr
ATTN: Doc. Con. for W. D. Barfield
ATTN: Doc. Con. for Reference Library
ATTN: Doc. Con. for W. M. Hughes
ATTN: Doc. Con. for E. W. Jones, Jr.
ATTN: Doc. Con. for John Zinn
ATTN: Doc. Con. for E. S. Bryant

University of California
Lawrence Livermore Laboratory
ATTN: G. R. Haugen
ATTN: A. Kaufman
ATTN: D. J. Wuebbles
ATTN: J. F. Tinney
ATTN: Julius Chang
ATTN: Tech. Info. Dept.
ATTN: W. H. Duewer

Sandia Laboratories
ATTN: Doc. Con. for W. D. Brown
ATTN: Doc. Con. for Org. 9220
ATTN: Doc. Con. for Craig Hudson
ATTN: Doc. Con. for J. C. Eckardt
ATTN: Doc. Con. for C. W. Gwyn
ATTN: Doc. Con. for D. A. Dahlgren
ATTN: Doc. Con. for M. L. Kramm
ATTN: Doc. Con. for T. Wright
ATTN: Doc. Con. for Charles Williams
ATTN: Doc. Con. for Sandia Rpt. Coll.
ATTN: Doc. Con. for Doc. Con. Div.

Sandia Laboratories
Livermore Laboratory
ATTN: Doc. Con. for Thomas Cook

Department of Energy
Div. of Hqs. Services, Library Branch, G-043
ATTN: Doc. Con. for D. Kohlstad
ATTN: Doc. Con. for J. D. LaFleur
ATTN: Doc. Con. for Class. Tech. Lib.
ATTN: Doc. Con. for George Regosa
ATTN: Doc. Con. for Rpts. Section
ATTN: Doc. Con. for R. Kandel
ATTN: Doc. Con. for H. H. Kurzweg

DEPARTMENT OF ENERGY (Continued)

Argonne National Laboratory
Records Control
ATTN: Doc. Con. for A. C. Wall
ATTN: Doc. Con. for S. Gabelnick
ATTN: Doc. Con. for J. Berkowitz
ATTN: Doc. Con. for Lib. Svsc. Rpts. Sec.
ATTN: Doc. Con. for Len Liebowitz
ATTN: Doc. Con. for David W. Green
ATTN: Doc. Con for Gerald T. Reedy

OTHER GOVERNMENT AGENCY

Department of Commerce
Office of Telecommunications
Institute for Telecom Science
ATTN: William F. Utlaut

DEPARTMENT OF DEFENSE CONTRACTORS

Aero-Chem Research Laboratories, Inc.
3 cy ATTN: A. Fontijn

Aerodyne Research, Inc.
ATTN: M. Camac
ATTN: F. Bien

Aerospace Corporation
ATTN: Harris Mayer
ATTN: Thomas D. Taylor
ATTN: R. D. Rawcliffe
ATTN: R. Grove
ATTN: R. J. McNeal

University of Denver
Colorado Seminary
Denver Research Institute
ATTN: Sec. Officer for Mr. Van Zyl
ATTN: Sec. Officer for David Murcray

General Electric Company
TEMPO-Center for Advanced Studies
ATTN: Warren S. Knapp
5 cy ATTN: DASIAC, Art Feryok

General Research Corporation
ATTN: John Ise, Jr.

Geophysical Institute
University of Alaska
ATTN: T. N. Davis
3 cy ATTN: Neal Brown

Honeywell Incorporated
Radiation Center
ATTN: W. Williamson

HSS Incorporated
ATTN: A. H. Tuttle

Institute for Defense Analyses
ATTN: Hans Wolfhard
ATTN: Ernest Bauer

DEPARTMENT OF DEFENSE CONTRACTORS (Continued)

Lockheed Missiles and Space Co. Inc.
ATTN: Billy M. McCormac, Dept. 52-54
ATTN: John B. Cladis, Dept. 52-12
ATTN: J. B. Reagan, Dept. 52-12
ATTN: John Kumer
ATTN: Martin Walt, Dept. 52-10
ATTN: Richard G. Johnson, Dept. 52-12
ATTN: Robert D. Sears, Dept. 52-14
ATTN: Tom James

Mission Research Corporation
ATTN: P. Fischer
ATTN: D. Archer

Photometrics, Inc.
3 cy ATTN: I. L. Kofsky/D. P. Villanucci/G. Davidson

Physical Dynamics, Inc.
ATTN: Joseph B. Workman

Physical Sciences, Inc.
ATTN: Kurt Wray

R & D Associates
ATTN: Robert E. Lelevier
ATTN: Forrest Gilmore

R & D Associates
ATTN: Herbert J. Mitchell

Science Applications, Inc.
ATTN: Daniel A. Hamlin

Space Data Corporation
ATTN: Edward F. Allen

SRI International
ATTN: M. Baron
ATTN: Ray L. Leadabrand
ATTN: Walter G. Chesnut

SRI International
ATTN: Warren W. Berning

Technology International Corporation
ATTN: W. P. Boquist

Utah State University
ATTN: D. Burt
ATTN: Kay Baker
ATTN: C. Wyatt
ATTN: Doran Baker

Visidyne, Inc.
ATTN: L. Katz
ATTN: William Reidy
ATTN: Henry J. Smith
ATTN: Charles Humphrey
ATTN: J. W. Carpenter
ATTN: T. C. Degges